

# **Characterisation of Single Photon Avalanche Detectors**



**Lim Zheng Jie**  
**A0102464R**

**Supervised by:**  
**Professor Christian Kurtsiefer**

**A thesis submitted for the Degree of  
Bachelor of Science with Honours in Physics**

**Department of Physics  
National University of Singapore**

## Acknowledgements

First of all, I would like to thank my supervisor Professor Christian Kurtsiefer for once again giving me the opportunity to work with the wonderful Quantum Optics group.

Thank you Hou Shun! For repetitively answering to my infinite curiosity, for the many many over-time, for the sacrifices of “dynamic time”, for the lack of sleep, for believing in me when I don’t even believe in myself, for many many things else, and most of all, thank you for your patience with me. I couldn’t thank you further. You are officially free from my annoyance!

A very special thanks to Victor for always being there for me. I definitely wouldn’t have survived both projects without your support.

Thank you Yi Cheng and Brenda for the support during the last few weeks of FYP. The report has been more awesome than ever because of your help!

Thank you Chi Huan; Life in CQT has been wonderful because of your accompany!

And thanks to the awesome social animals in 01-04! For the many carbon dioxide and oxygen we have shared.

Last but not least, to each and everyone in the group, thank you for an awesome one year!

Graduate lo!

# Contents

<b>Abstract</b>	<b>iv</b>
<b>1 Introduction</b>	<b>1</b>
<b>2 Understanding the Avalanche Photodiode</b>	<b>5</b>
2.1 Photodiode working principle . . . . .	5
2.1.1 P-N junction . . . . .	5
2.1.2 Operation mechanism . . . . .	6
2.1.3 P-I-N junction . . . . .	7
2.2 Avalanche photodiode working principle . . . . .	7
2.2.1 Diode structure . . . . .	8
2.2.2 Electric field distribution . . . . .	9
2.2.3 Avalanche multiplication . . . . .	9
2.3 Quenching circuits . . . . .	9
2.3.1 Passive quenching circuit . . . . .	10
2.3.2 Active quenching circuit . . . . .	11
<b>3 Characterisation of avalanche photodiodes</b>	<b>12</b>
3.1 Avalanche photodiodes of interest . . . . .	12
3.1.1 Home-built APD . . . . .	12
3.1.2 Commercial APD . . . . .	14
3.2 Breakdown voltage, Pulse height, and Dark counts . . . . .	15
3.2.1 Experimental setup . . . . .	15
3.2.2 Breakdown voltage . . . . .	16
3.2.3 Pulse height . . . . .	18
3.2.4 Dark count . . . . .	22
3.3 Detection Efficiency . . . . .	25
3.3.1 Experimental setup . . . . .	25
3.3.2 Dependence with overvoltage . . . . .	28
3.3.3 Dependence with count rate . . . . .	30
3.4 Timing Jitter . . . . .	32
3.4.1 Experimental setup . . . . .	32
3.4.2 Dependence with count rate . . . . .	34
3.4.3 Dependence with overvoltage and temperature . . . . .	35
3.5 Breakdown Flash Probability . . . . .	39

3.5.1	Experimental setup . . . . .	39
3.5.2	Quantifying Breakdown Flash Probability . . . . .	40
<b>4</b>	<b>Conclusion and outlook</b>	<b>41</b>

## **Abstract**

In this work, we investigate the performance of various single photon avalanche detectors (SPAD) in the Geiger mode, namely passively quenched Perkin Elmer C30902SH and Laser Components SAP500, and actively quenched Perkin Elmer SPCM-AQR-15 and MPD PD-050-CTD-FC. The performance characteristics that are examined include: breakdown voltage, pulse height, dark count rate, detection efficiency, timing jitter, and breakdown flash probability. We conclude that the Laser Components SAP500 offers better combination of detection efficiency, low dark counts, and timing precision as compared to the Perkin Elmer C30902SH.

# 1 Introduction

The most widely remembered part of Einstein's 1905 paper on the quantum theory was his explanation of the photoelectric effect. The photoelectric effect was first discovered by the German physicist, Heinrich Hertz, in 1887 when he noticed that a charged object loses its charge more readily when illuminated by ultraviolet light [1]. It remained unexplained until 1905 when Albert Einstein postulated the existence of light as discrete bundles of energy called quanta, now referred to as photons [2]. Einstein's theory predicts that when a beam of light is incident on the surface of a metal, a quanta of energy will be absorbed completely by an electron, which suggests that electrons can only absorb the energy of light in discrete energy quanta regardless of the intensity of the incident light [3].

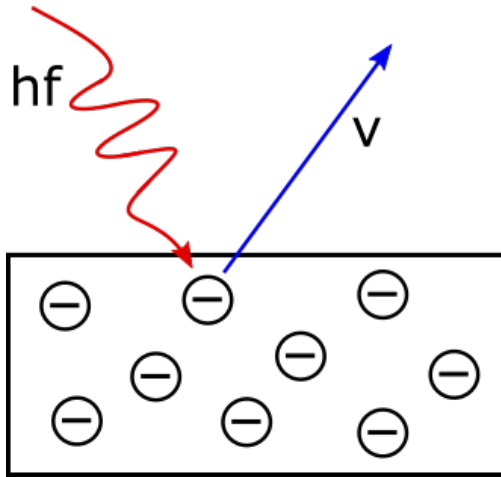


Figure 1: Illustration of the photoelectric effect. Electron is ejected with velocity  $v$  when incident upon by a photon of energy  $hf$ .

The kinetic energy ( $E$ ) of the electron once it has escaped from the material is directly proportional to the photon's frequency. These electrons are also termed as photoelectrons.

$$E = \frac{1}{2}mv^2 = hf - W \quad (1)$$

where,

$h$  is the Planck constant

$f$  is the frequency of light

$W$  is the work function (minimum energy of photon required to free the electron)

The energy of a single photon depends on its wavelength, where photons in the visible or near-infrared range have energy in the order of  $10^{-19}$  J, which were undetectable by the earlier forms of light sensors. However, the detection of low intensity light was made possible when the first

photoelectric tube (PET) was invented by Elster and Geiter over a century ago in 1913 [4], exploiting the photoelectric effect using visible light to strike alkali metals (potassium and sodium). Over two decades later, RCA laboratories produced the first photomultiplier tube (PMT), which marks the start of single photon detection [4].

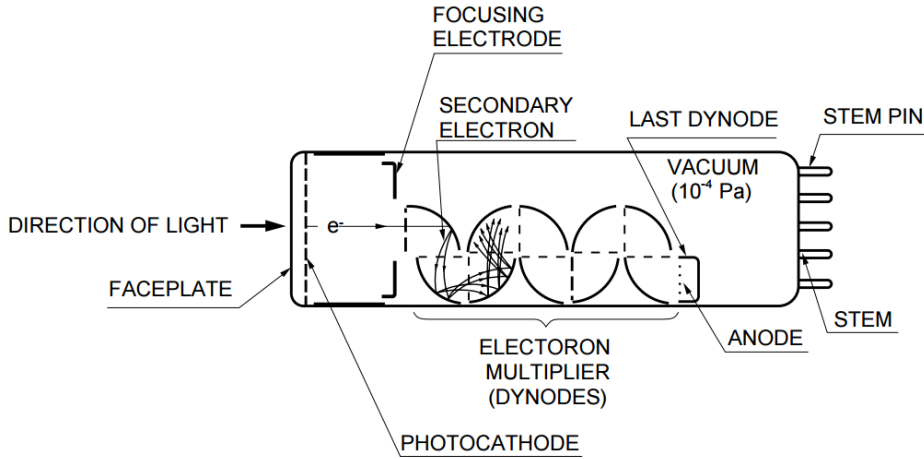


Figure 2: The sketch of a photomultiplier tube. A typical PMT is made up of a photoemissive cathode (photocathode) followed by focusing electrodes, an electron multiplier (dynode) and an electron collector (anode) in a vacuum tube. [5]

In a PMT, when light enters the photocathode, one or more photoelectrons are emitted into the vacuum. These photoelectrons are then accelerated by the focusing electrode voltages towards the electron multiplier (dynode) where electrons are multiplied through the process of secondary emission and are collected at the anode as an output signal. Due to secondary emission which leads to an overall gain (electron multiplication), PMTs possess extremely high sensitivity relative to other photosensitive devices used to detect light in the ultraviolet, visible, and near infrared regions. However, PMTs are very sensitive to magnetic fields and its cost of production is high due to the complicated mechanical structure inside the vacuum container [4]. Thus, PMTs were unable to fulfil the needs of many modern experiments such as those in high-energy physics which involves strong magnetic fields. This triggered the exploration for alternatives to PMTs.

Development in photodetection soon shifted to the exploration of solid state semiconductor detectors which exploits the idea of a p-n junction in the semiconductor material (to be discussed in detail in the next chapter). One successful innovation is the PIN photodiode<sup>1</sup> which delivers high speed response when operated with a reverse bias. However, the PIN photodiode does not have any gain, which makes it unsuitable for low intensity light applications. Avalanche Photodiode (APD) were then developed which possesses high internal gain through the process of avalanche

---

<sup>1</sup>Refer to Section 2.1.3

multiplication that improves the signal-to-noise ratio<sup>2</sup>. However, the excess noise caused by extremely high reverse bias as well as the fluctuation of the avalanche multiplication limits the useful range of the gain [4].

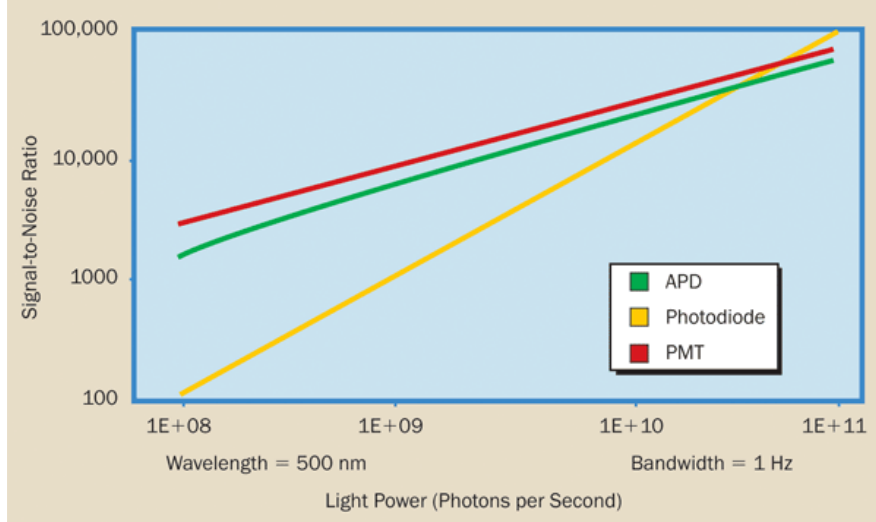


Figure 3: Signal-to-noise ratio versus light power for a typical PMT, APD, and photodiode.[6]

From Figure 3, we see that in general, the PMT performs best in extremely low light-level conditions in UV to near-IR wavelength ranges, ideally suited for fluorescence spectroscopy. Photodiodes perform better in higher light levels in the UV to near-IR range, making it useful as an optical power meter. The APD on the other hand, performs best in applications involving low light levels and high-bandwidth applications conducted in the near-IR wavelength range, suitable for applications such as photon counters. Therefore, each photodetector has its own practicality in different areas - no one photodetector is absolutely better than the other.

Photon counting techniques are used in various areas of industry, research and communication technologies. Specific applications include the incorporation of single photon detectors in Quantum Information Technologies (QIT), where experiments focus on studying photonic state manipulation at the quantum level [7]. QIT has received a lot of attention over the years for its potential to revolutionize many areas of science and technology [8]. The most mature of these innovations is Quantum Key Distribution (QKD), more widely known as Quantum Cryptography, which uses quantum mechanics to guarantee secured communication [9]. However, there still are several explicit limits on experimental QKD associated with the dependence of these applications on optical components such as single photon detectors [10] [8]. Unless significant improvements are made in terms of detector performance, there will always be loopholes in the credibility of the QKD system.

---

<sup>2</sup>A measure that compares the level of a desired signal to the level of background noise.

The performance of a single photon detector should be assessed in terms of its spectral range, dead time, dark count rate, detection efficiency, and timing jitter. The specific requirements of the photon detector's performance differ considerably for different experiments, and various parameters are not always complementary. For example, in single photon scattering experiments [11] where optical signals are weak, the desirable characteristics of a photon detector would be high efficiency and low dark counts. On the other hand, experiments such as null stellar intensity interferometry [12] which require sub-milliarcsecond resolution would require photon detectors with very low timing jitter. Judging from the above criteria, PMTs are not a favourable choice in many such experiments. Not only do PMTs have very low quantum efficiency and high noise in longer wavelength ranges, they also require high operating voltages (1000 to 2000 volts) to accelerate electrons within the chain of dynodes. Thus, they are slowly being replaced by APDs as the state-of-the-art tool for single photon detection.

In this thesis, we will examine some of these characteristics in detail, with reference to the requirements of the different applications in our quantum optics lab. Specifically, we will be looking into the breakdown voltage, pulse height, dark count rate, detection efficiency, timing jitter, and breakdown flash probability of various APDs. In addition, this thesis will outline accurate measurement strategies for characterizing APDs, and subsequently make a comparison between the APDs' performances.

## 2 Understanding the Avalanche Photodiode

### 2.1 Photodiode working principle

A photodiode is a semiconductor device that converts light into current. The current is generated when photons are absorbed in the photodiode. It exploits the electronic properties of semiconductor materials, principally silicon (S), germanium (Ge), and gallium arsenide (GaAs), as well as organic semiconductors. The property of these semiconductor materials can be manipulated by the addition of impurities, otherwise known as doping.

#### 2.1.1 P-N junction

Figure 4 illustrates the principle of a p-n junction.

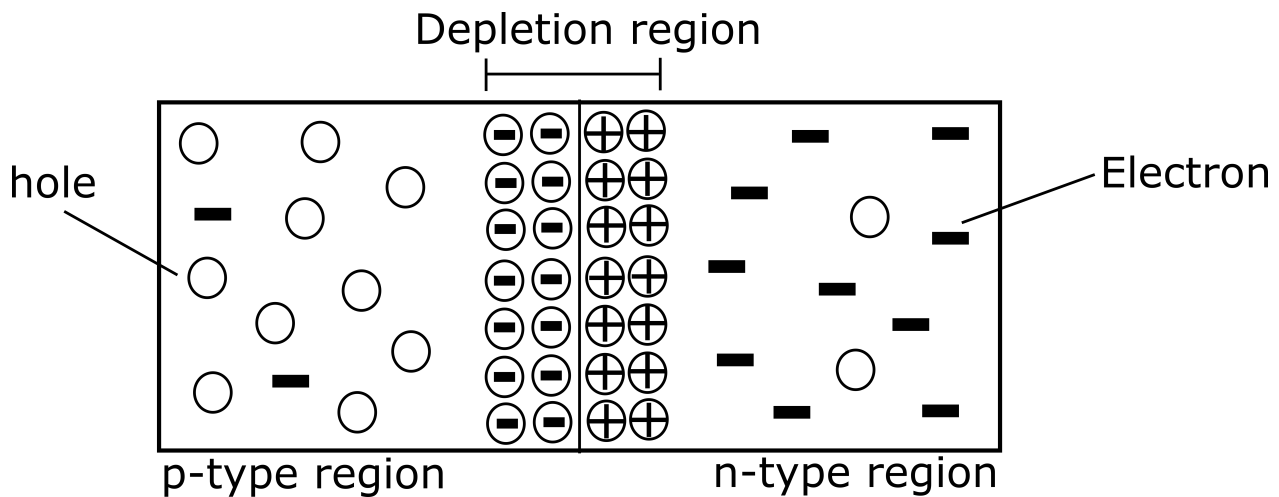


Figure 4: A p-n junction is formed by joining n-type and p-type semiconductor materials, where n-type is a region of excess free electrons and p-type is a region of excess holes. When both regions are in contact, the electrons and holes recombine at the junction to form a depletion region.

Doping a semiconductor material with a small amount of impurities, such as phosphorus (P) or boron (B), greatly increases the number of free electrons or holes (charge carriers) within the semiconductor. When a doped semiconductor contains excess holes it is called 'p-type', and when it contains excess free electrons it is known as 'n-type'.

A p-n junction is formed by joining n-type and p-type semiconductor materials. When both regions are in contact, diffusion of charge carriers occurs. Electrons move towards the p-type region while holes move towards the n-type region, and they recombine at the junction to form a depletion region. A potential difference is simultaneously created across the depletion region

with the positive potentials at the n-type region and negative potential at the p-type region, as illustrated in Figure 4.

### 2.1.2 Operation mechanism

When photons of energy greater than the bandgap of silicon (approximately 1.14 eV) are illuminated onto the photodiode, they are absorbed and free charge carriers are created.

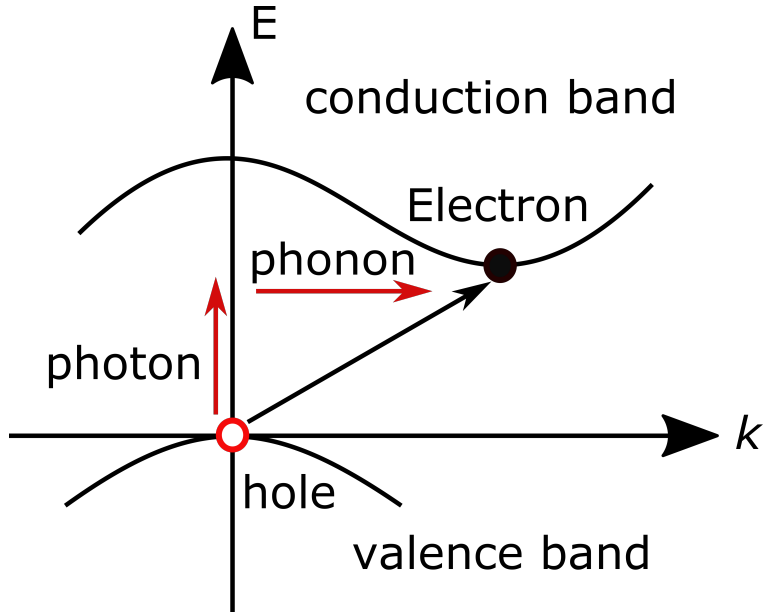


Figure 5: Band structure of silicon showing the indirect band gap. An incident photon of energy greater than the band gap of silicon creates an electron in the conduction band and a hole in the valence band, at the same time fulfilling the conservation of momentum by the additional absorption of a phonon.

The separated electron and hole are then attracted by the positive and negative terminals respectively, and this movement generates a flow of external current. However, if the created charge carriers of that region recombine with the bulk carriers of the same region, the carriers are lost and no external current flows.

By applying a reverse bias voltage with the negative terminal at the p-type side and positive terminal at the n-type side as shown in Figure 6, the potential difference across the depletion region is increased. Thus, the created electrons and holes are rapidly separated and swept out of the depletion region to create a photocurrent.

### 2.1.3 P-I-N junction

To allow for faster detection, a sufficiently large area in which the photons can be collected and converted is required. This can be achieved by adding an intrinsic (undoped) area in between the p-type and n-type regions to create a PIN junction.

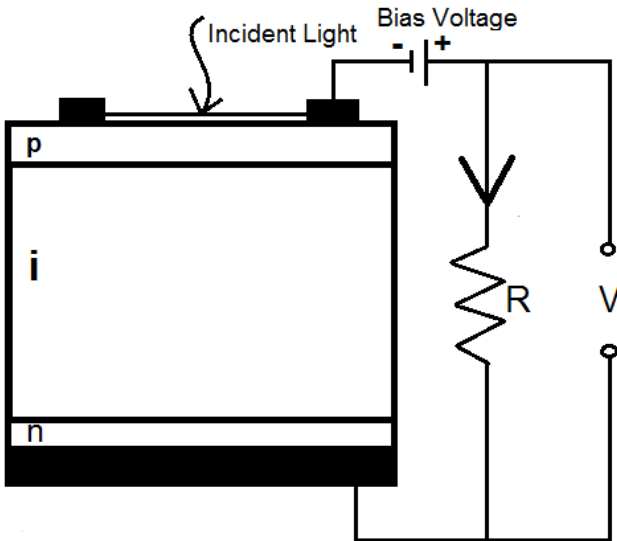


Figure 6: Cross section of the PIN photodiode, showing the intrinsic region between the p-type and n-type regions. The PIN photodiode operates in the photoconductive mode when a reverse bias is applied.

The intrinsic region serves to increase the width of the depletion region by providing a larger area where the electron-hole pairs can be created. This in turn provides for more efficient conversion of photons to charge carriers, thus increasing the level of responsivity.

## 2.2 Avalanche photodiode working principle

The Avalanche Photodiode (APD) possesses a similar structure to that of the PIN photodiode, and operates at a much higher reversed bias state as shown in Figure 7. This property enables a single photon to induce a significant avalanche of electrons. This operation regime is called the single-photon avalanche mode or the Geiger mode. In this mode, the APD is used as a trigger device which allows for the detection of low intensity light (down to the single photon level). In addition, this means that the APD offers very high levels of gain (in the order of  $10^7$ ) thus providing a much greater level of sensitivity.

### 2.2.1 Diode structure

Most commonly available APDs are fabricated from silicon and employ a “reach-through” structure as shown in Figure 7.

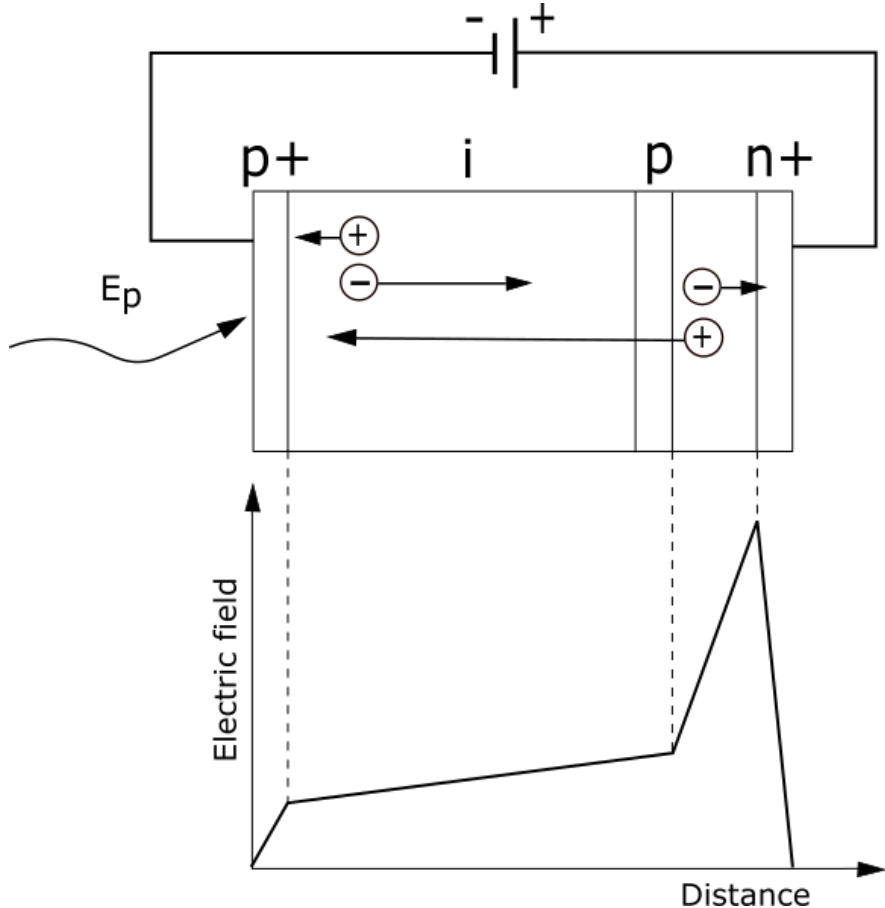


Figure 7: A schematic illustration of the reach-through structure of an avalanche photodiode biased for an avalanche gain. n+ represents a layer of highly doped n-type region; p+ represents a layer of highly doped p-type region; p represents a layer of lightly doped p-type region; i represents an intrinsic (or undoped) layer. The figure below shows the electric field at the respective regions of the APD.

The basic design of a reach-through APD consists of a thin region of high electric field where the avalanche takes place, and a thick substrate region of very low electric field. If the photon strikes from the n+ side, the APD will be sensitive to wavelengths ranging from 450 nm to 1000 nm, such as the Hamamatsu S6045 series. If the photon strikes from the p+ side, the APD will then exhibit sensitivity to the wavelength range of 200nm to 800nm, such as the Hamamatsu S8664 series [13].

## 2.2.2 Electric field distribution

When a reverse bias is applied, a depletion region is formed in between the highly doped n+ and lightly doped p layers, as shown in Figure 7. Since the n+ layer is more highly doped, the voltage required to deplete the intermediate layer is rather high. Thus, a high electric field is created in the region between the n+ to p-layer. Since doping beyond the p-layer is low, depletion beyond the p-layer requires less voltage, thus electric field are lower in that region.

## 2.2.3 Avalanche multiplication

With reference to Figure 7, when a photon strikes from the p+ side, an electron hole pair is created in the intrinsic region. Under the influence of the electric field, the electrons move towards the high electric field region and gain kinetic energy. If the electron gains sufficient energy, collision with atoms in the crystal lattice will create more free electron hole pairs through impact ionization. The process repeats and causes further ionization resulting in a gain in the number of free electron holes pairs generated for a single incident photon. This triggers an avalanche breakdown, where multiplication of free electrons and holes ultimately results in a sustained avalanche.

## 2.3 Quenching circuits

During an avalanche, an exponentially growing number of electrons is generated, producing a current spike within a few picoseconds. If the avalanche is not quenched, it will continue to go on, and no further photons can be detected. Therefore, an external electric circuit is used to quench the APD by lowering the bias voltage below the breakdown voltage, and the APD quickly resumes to its non-conducting state. To detect another photon, the APD have to be recovered back to its conducting state by raising the bias voltage above breakdown so that another ionizing event can take place.

This operation requires a suitable circuit that satisfies the following requirements:

- 1) Sense the leading edge of the avalanche current
- 2) Generate an output pulse that is well synchronised in time to the avalanche rising edge
- 3) Quench the avalanche by lowering the reversed bias below breakdown voltage
- 4) Restore the APD to its conducting state

Here, we discuss the following two quenching strategies.

### 2.3.1 Passive quenching circuit

This is the simplest and most common method for quenching an avalanche. Figure 8 illustrates a basic passive quenching circuit which uses a current limiting ballast resistor ( $R_B$ ).

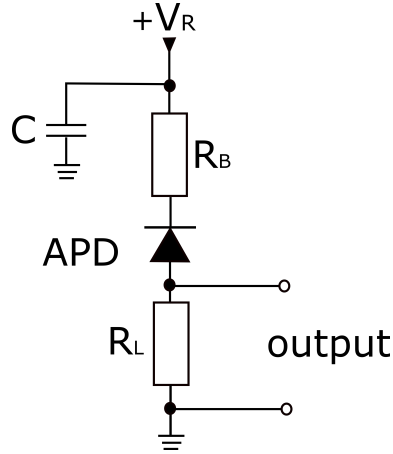


Figure 8: A schematic of a basic passive quenching circuit for an APD. The APD is connected in series with a comparatively large ballast resistor, with an applied bias voltage across the series arrangement.

Here, we define the overvoltage ( $V_{OV}$ ) as the difference of the reverse bias voltage ( $V_R$ ) and the breakdown voltage ( $V_{BR}$ ), i.e.

$$V_{OV} = V_R - V_{BR} \quad (2)$$

Prior to photon absorption, the APD is in the non-conducting state - no current flows. When a photon is absorbed, an avalanche occurs and the APD enters the conducting state. The current flowing through the APD is limited by  $R_B$ , and is given by

$$I = \frac{V_{OV}}{R_B} \quad (3)$$

To continue to be in the conducting state after an avalanche, the current ( $I$ ) passing through the APS must be higher than  $I_{latch}$ , such that there is always an electron or hole in the avalanche region [14]. However, to achieve quenching effects,  $I$  should be much less than  $I_{latch}$  so that the avalanche current can quickly discharge the junction capacitance ( $C$ ) until the voltage across the APD drops below  $V_{BR}$ , returning it to the non-conducting state. For C30902SH,  $I_{latch} = 50 \mu\text{A}$ . The time taken for the APD to recover to its initial non-conducting state is given by the time constant of the effective RC circuit, i.e.

$$\tau = R_B C \quad (4)$$

For C30902SH, with  $C = 1.6 \text{ pF}$  and  $R_B = 390 \text{ k}\Omega$ , a dead time of  $0.62 \mu\text{s}$  is calculated.

### 2.3.2 Active quenching circuit

The active quenching circuit is designed to reduce the dead time significantly when operating at a high  $V_{OV}$ . It operates by temporarily dropping the  $V_R$  for a fraction of a microsecond upon detection of an avalanche and then reapplying a high  $V_R$ . Immediately after the voltage drop, since  $V_R$  is lower than  $V_{BR}$ , the APD is free of charge carriers hence no avalanche can occur. The higher voltage is subsequently reapplied, allowing rapid recovery of the APD to the conducting state through a small load resistor. The whole process results in a dead time of approximately 50 ns, much faster than that of the passive quenching circuit.

### 3 Characterisation of avalanche photodiodes

#### 3.1 Avalanche photodiodes of interest

In this thesis, we will be looking at the characteristics of four different types of APDs, two of which are home-built APDs, while the other two are commercial APDs. The aim is to investigate breakdown voltage, dark counts, pulse height, breakdown flash, detection efficiency, and timing jitter, and to make a comparison between the various APDs.

##### 3.1.1 Home-built APD

The Perkin Elmer C30902SH and Laser Components SAP500 are used in customisable APD units that adopt a passive quenching circuit.

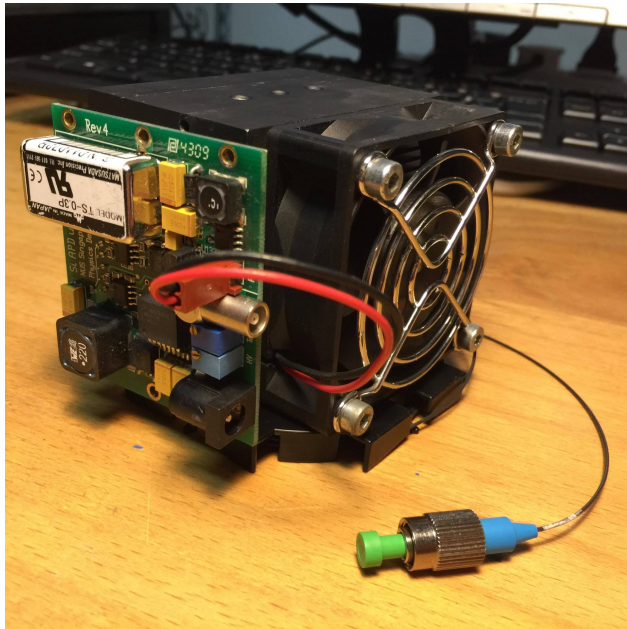


Figure 9: Exterior of a complete Perkin Elmer C30902SH unit that consists of a fibre pigtail, a circuit board, and a fan to cool the unit.

The whole APD unit is made up of heat sink that contains a 3-stage peltier element and a cooling block that houses the diode, thermistor, and fibre as shown in Figure 10.

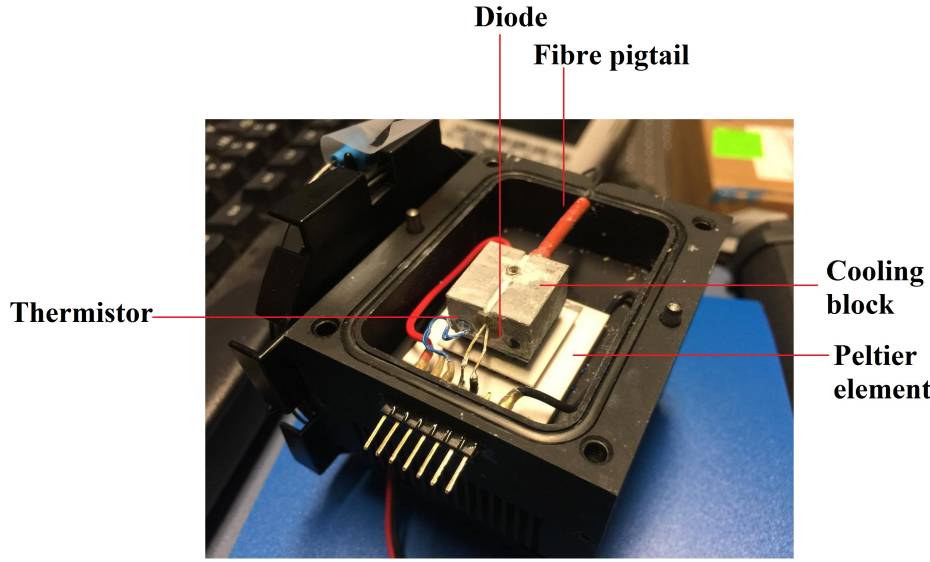


Figure 10: Interior of an APD unit which consists of a 3-stage peltier element and a cooling block that houses the diode, thermistor, and fibre.

### Temperature sensing

The temperature of the APD is set and stabilized by adjusting the peltier element current, and is measured by the thermistor. The temperature of the APD can be obtained from the thermistor resistance via the Steinhart-Hart equation, given by

$$\frac{1}{T} = A + B \ln(R) + C[\ln(R)]^3 \quad (5)$$

where,

T is the temperature (in Kelvins)

R is the resistance of the thermistor (in Ohms)

A, B, C are the SteinhartHart coefficients which varies for different types of thermistor.

The SteinhartHart equation is a model of the resistance of a thermistor at different temperatures. The thermistor has a nominal resistance of  $10\text{ k}\Omega$  at  $298.15\text{ K}$ . The resistance of the thermistor is converted into a measured voltage by making it part of a potential divider with a reference voltage of  $10\text{ V}$ , with the upper leg of that divider chosen to have a resistance of  $100\text{ k}\Omega$ . With that, we obtain values of the Steinhart-Hart coefficients. At an operating temperature of approximately  $-20^\circ\text{C}$ , the thermistor delivers an output voltage of  $5.18\text{ V}$ .

## APD electronics

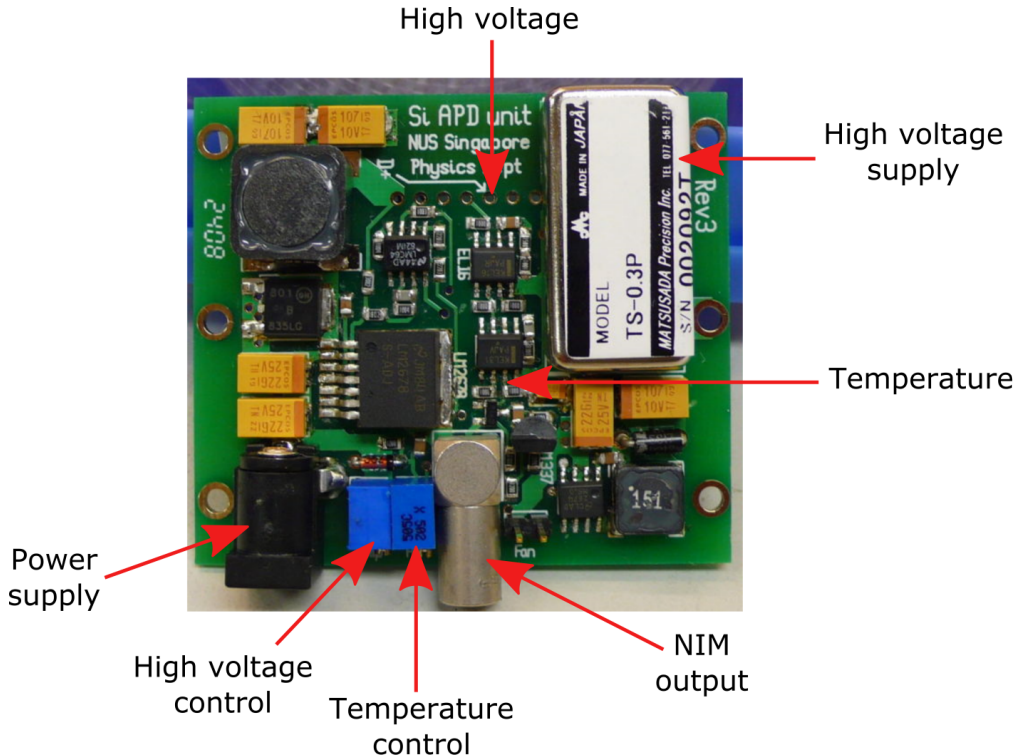


Figure 11: Circuit board to operate the APD

The APD circuit board generates a NIM-compatible output signal upon a photodetection event with a duration of about 15 ns, with the leading edge of this pulse being the relevant shoulder for timing measurements. The circuit board runs on a 12V DC supply and provides the high voltage bias to the APD, a NIM signal processing chain and a temperature control circuit. The peltier element requires 10 to 15 W of input power to cool the APD to a temperature of -15 to -35 °C.

### 3.1.2 Commercial APD

The commercial APDs used are the Perkin Elmer SPCM-AQR-15 and Micro Photon Devices PDM-050-CTC-FC, both of which are of a “reach-through” structure and adopt an active quenching circuit. Since these are commercial APDs, we are unable to customise any of the operating parameters of the APDs.

## 3.2 Breakdown voltage, Pulse height, and Dark counts

### 3.2.1 Experimental setup

A schematic of the setup that is used for this part of measurements is shown in Figure 12.

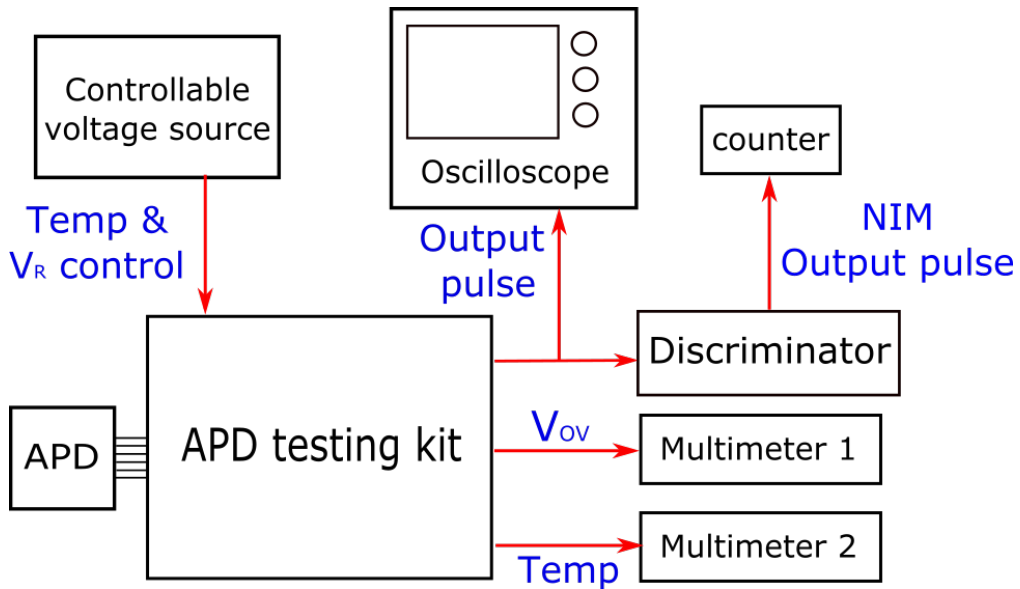


Figure 12: Setup for breakdown voltage, pulse height, and dark counts measurements.

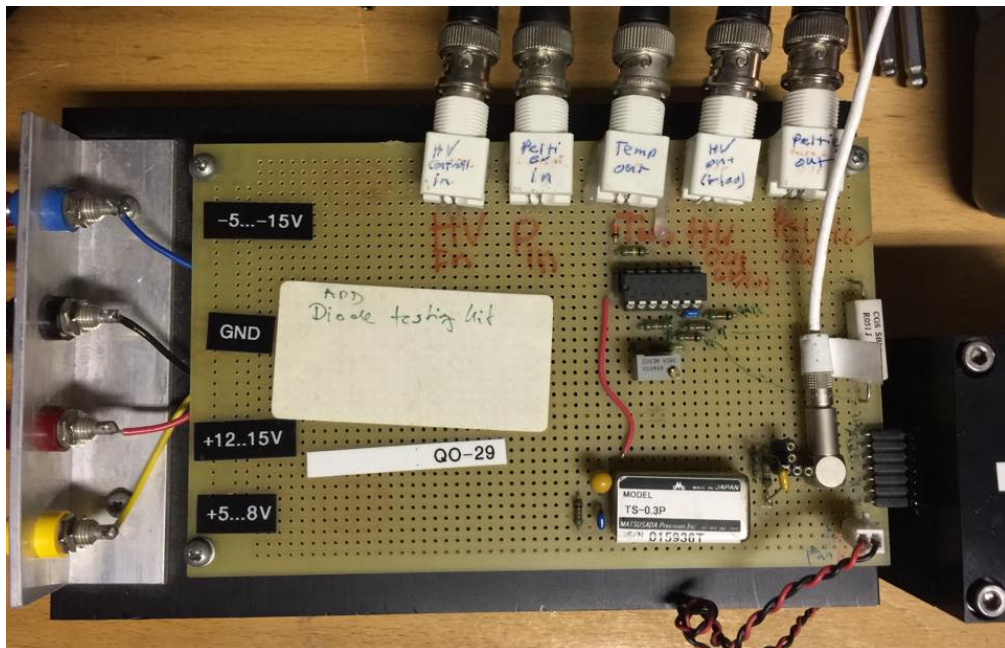


Figure 13: APD testing kit

Instead of the circuit board shown in Figure 11, the APD testing kit is used to operate the APD.

The APD testing kit is a simpler version of the circuit board where it does not have a discriminator to transform the signal into a NIM-compatible pulse. In addition, the APD testing kit is designed to allow convenience when varying the temperature and reversed bias voltage supplied to the APD of interest.

### 3.2.2 Breakdown voltage

In general, the breakdown voltage is defined as the minimum voltage that causes a portion of a material to become electrically conductive. In the context of diodes, the breakdown voltage ( $V_{BD}$ ) is defined as the minimum reverse voltage to make the diode conduct in reverse. As illustrated in Figure 14, the breakdown voltage corresponds to the point where the avalanche breakdown occurs.

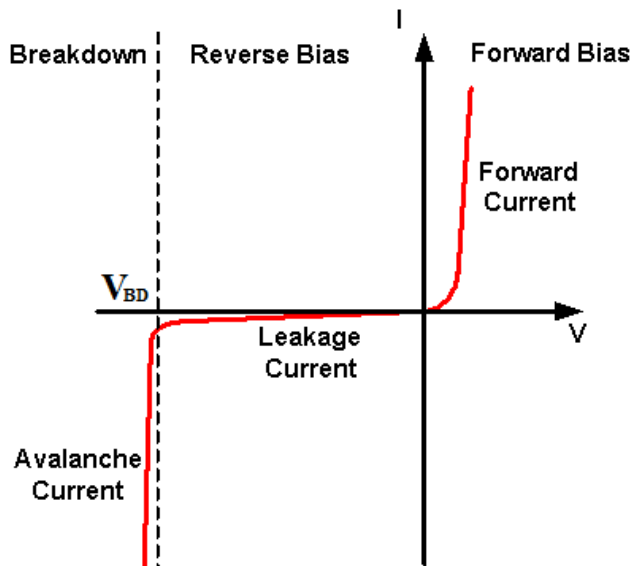


Figure 14: The current-voltage relationship of a diode

Using the setup as shown in Figure 12, the bias supplied to the APD is slowly increased until a pulse is seen on the oscilloscope, as shown in Figure 15. No light was sent to the input of the fibre coupled APD. We define the bias voltage at this point as the breakdown voltage.

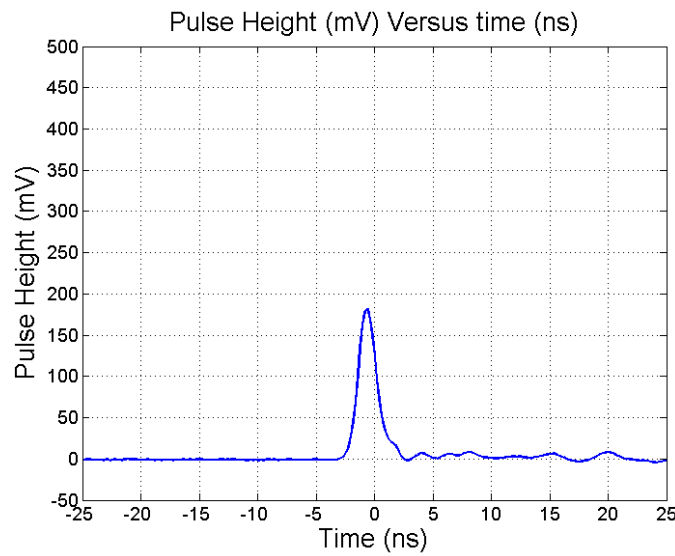


Figure 15: Breakdown pulse from Laser Components SAP500 as seen from the oscilloscope at  $V_{BR}$ . The pulse is triggered at the level slightly above the noise.

### Dependence with temperature

By making adjustments to the controllable voltage source, the temperature of the APD is varied from  $-30^{\circ}\text{C}$  to  $30^{\circ}\text{C}$  and the corresponding  $V_{BR}$  are measured.

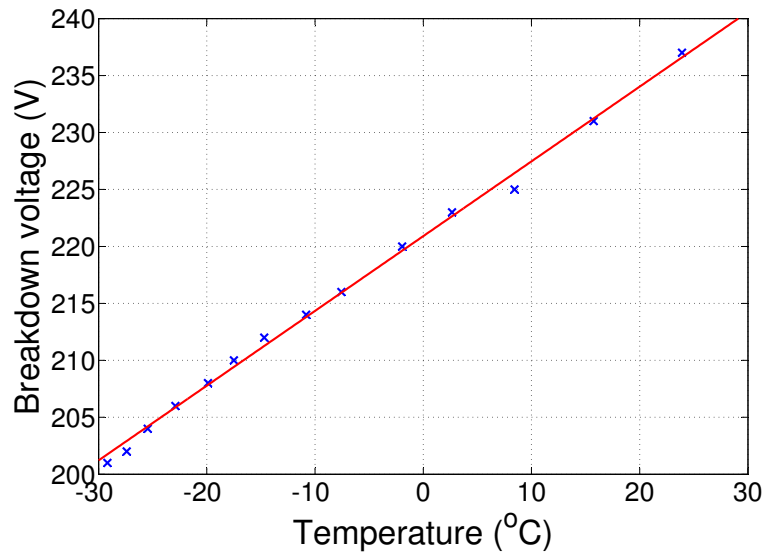


Figure 16: Breakdown voltage as a function of temperature for Perkin Elmer C30902SH.

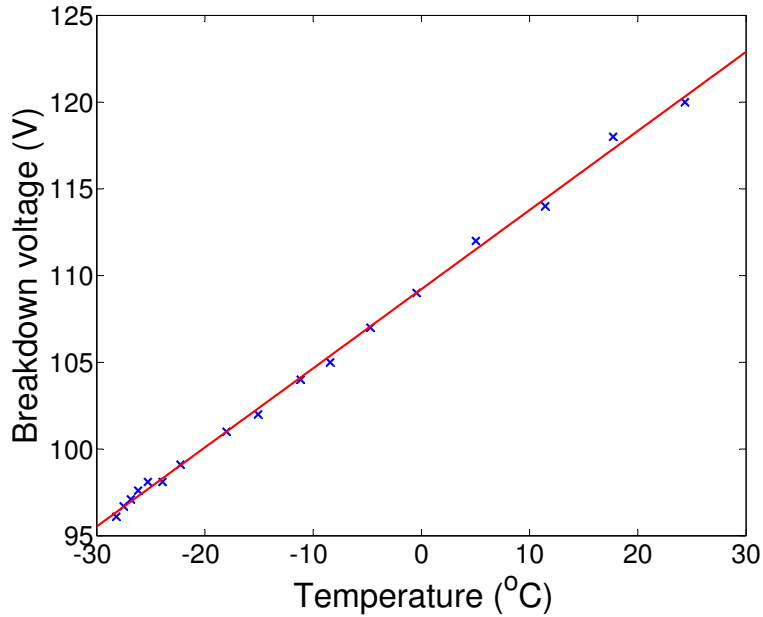


Figure 17: Breakdown voltage as a function of temperature for Laser Components SAP500.

The results shows that both APDs have breakdown voltages that varies fairly linearly with temperature. We can also see that SAP500 generally requires a lower breakdown voltage than that of Perkin Elmer C30902SH.

### 3.2.3 Pulse height

The pulse height of the APD corresponds to the multiplication gain ( $G$ ), where a higher pulse amplitude implies a higher gain.  $G$  is defined as the number of photoelectrons created per incident photon. The gain can be obtained from

$$G = \frac{1}{R_s e} \int_0^\infty V(t) dt \quad (6)$$

where,

$V(t)$  is the amplitude of the pulse in Volts.

$R_s$  is the resistor of the passive quenching circuit as shown in Figure 8.

Using the setup as shown in Figure 12, the mean pulse height is measured from the bottom of the pulse to the top of the pulse as seen on the oscilloscope.

## Dependence with overvoltage

With the APD set to an operating temperature of  $-20^{\circ}\text{C}$ , the mean pulse height are measured at overvoltages ranging from 0 to 30 V in steps of 3 V.

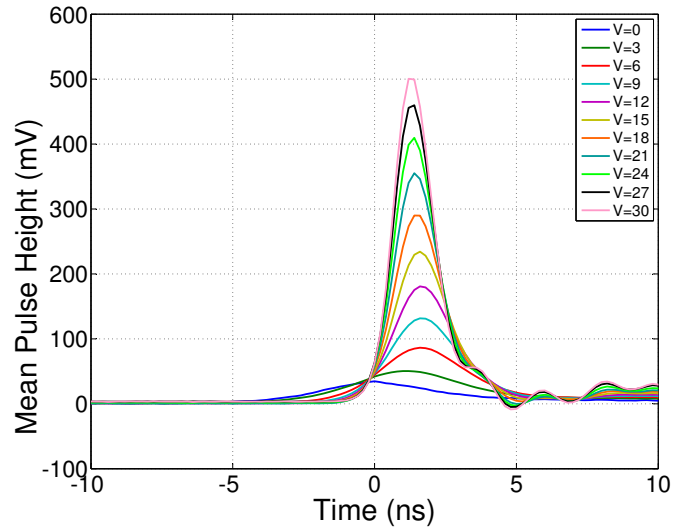


Figure 18: Mean pulse height as a function of time at varying overvoltages for Perkin Elmer C30902SH.

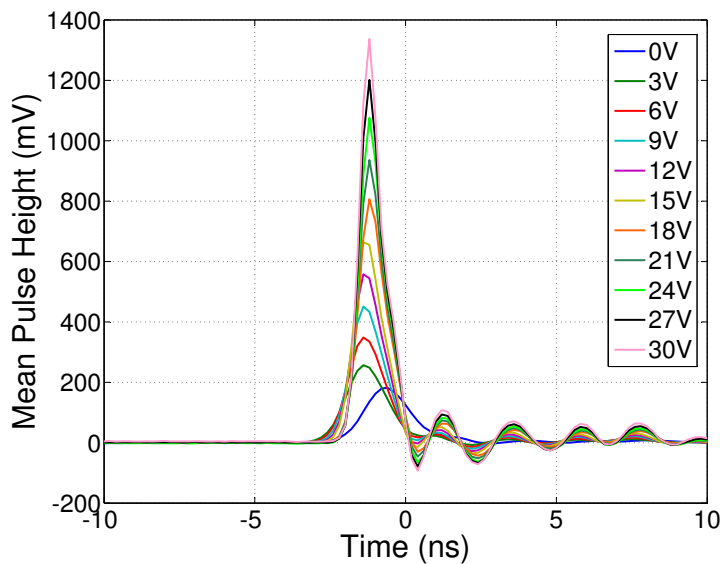


Figure 19: Mean pulse height as a function of time at varying overvoltages for Laser Components SAP500.

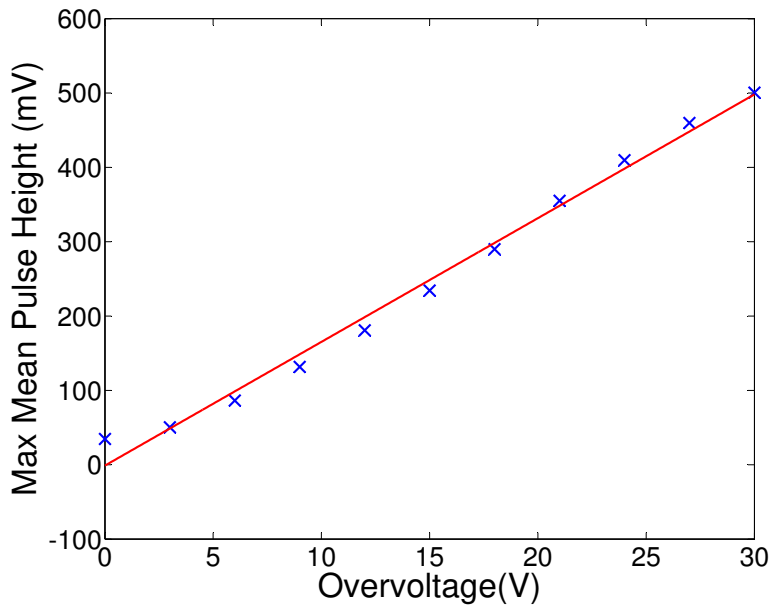


Figure 20: Maximum mean pulse height as a function of overvoltage for Perkin Elmer C30902SH.

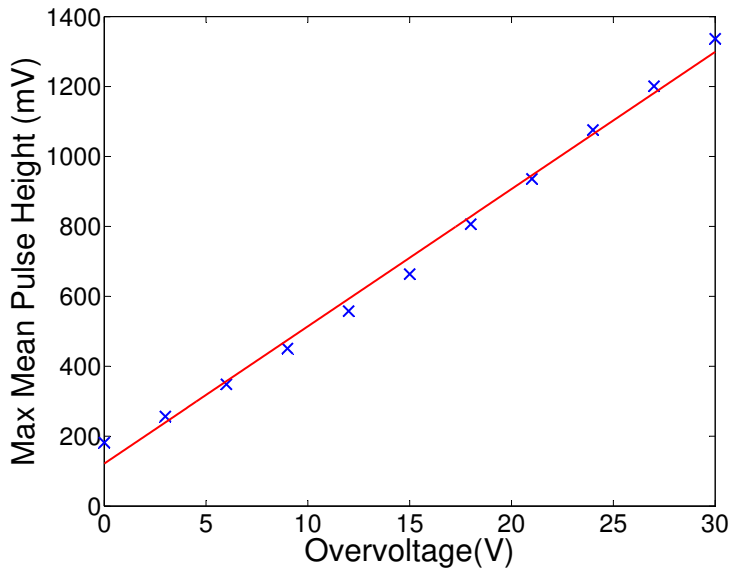


Figure 21: Maximum mean pulse height as a function of overvoltage for Laser Components SAP500.

The results shows that SAP500 produces a much narrower and higher-peaked pulse than C30902EH, which implies that the former has a higher responsivity and sensitivity than the latter.

The mean pulse heights are then converted into gain through Equation 6.

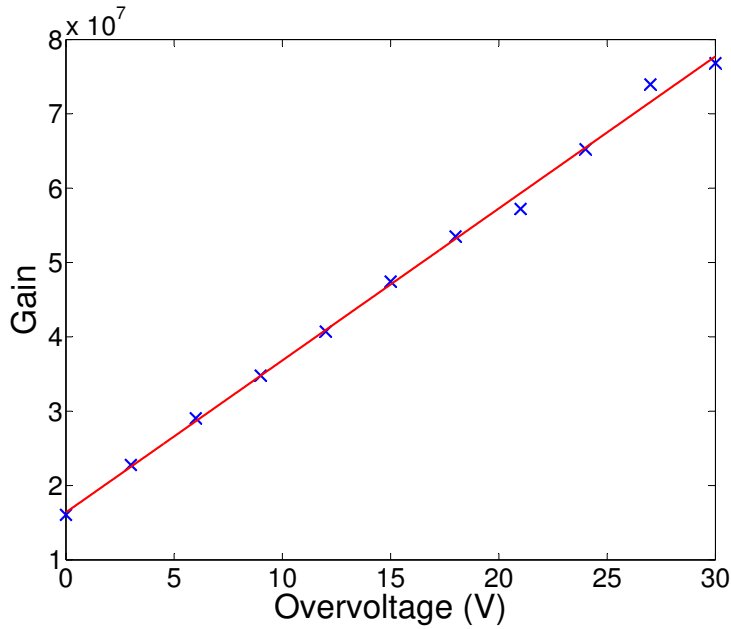


Figure 22: Gain as a function of overvoltage for Perkin Elmer C30902SH.

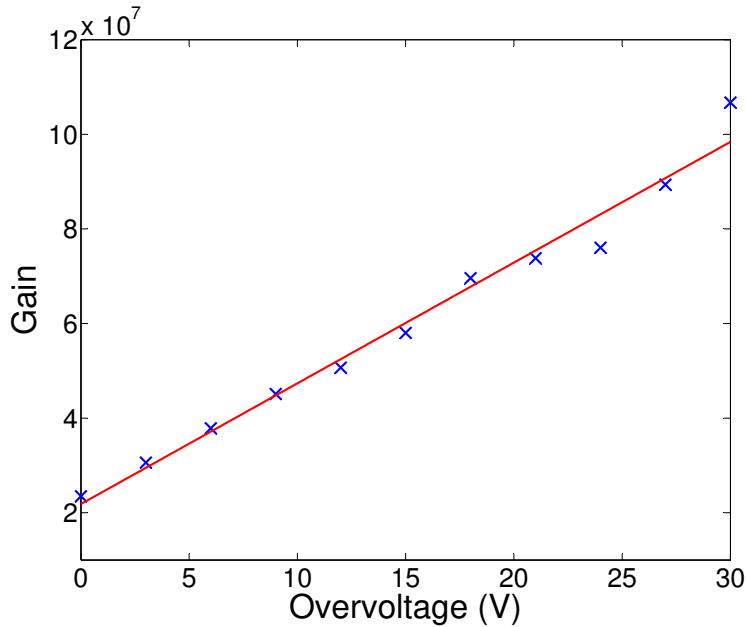


Figure 23: Gain as a function of overvoltage for Laser Components SAP500.

The gain of both APD increases with increasing overvoltage, and are fairly similar in the order of  $10^7$ .

### 3.2.4 Dark count

Dark counts are the response of photonic detectors in the absence of light. The dark count rate includes primary and secondary pulses. Primary dark pulses are the result of thermal energy exciting electrons and triggering avalanches as if they were real photon events [15]. A high  $V_{ov}$  also contribute to the primary dark pulses for it increases the electric field across the junction and raises the rate of avalanche. Secondary dark pulses are created due to afterpulsing effects. Afterpulsing occurs when the charge carriers are released after being trapped in the avalanche region [16]. These released charge carriers then retrigger avalanche breakdown which generates afterpulses. Afterpulsing increases with delay of avalanche quenching and with the current intensity, which is proportional to the overvoltage  $V_{ov}$  [17].

Using the setup as shown in Figure 12, the dark counts is registered by a counter for a period of 60s. The dark count rate ( $s^{-1}$ ) is obtained by averaging the total dark counts measured.

#### Dependence with overvoltage

With the APD set to an operating temperature of  $-20^{\circ}\text{C}$ , the dark count rates are measured at overvoltages ranging from 0 to 30V in steps of 3V.

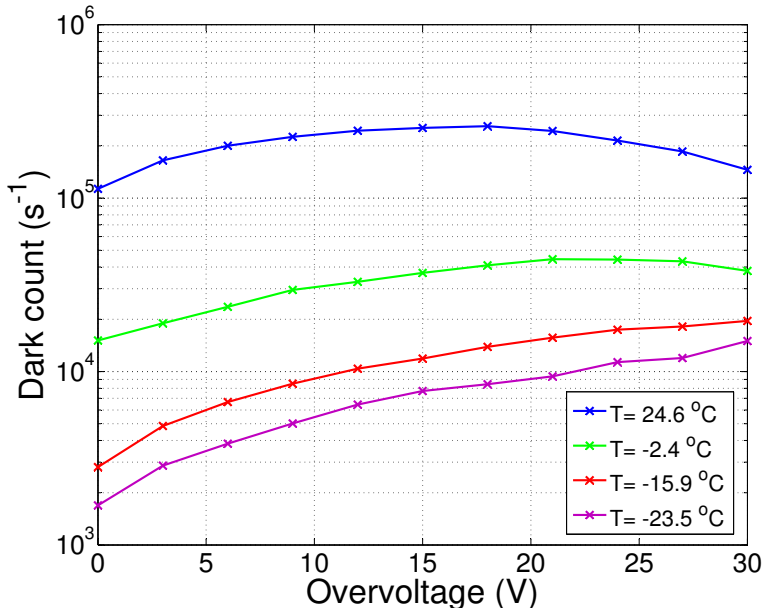


Figure 24: Dark count as a function of overvoltage at respective temperatures for Perkin Elmer C30902SH.

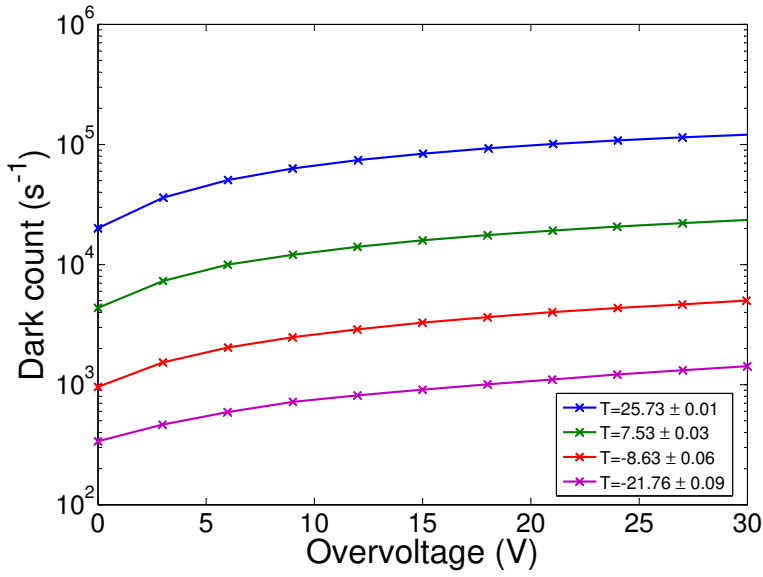


Figure 25: Dark count as a function of overvoltage at respective temperatures for Laser Components SAP500.

We can see that the dark count rate for SAP500 is lower than that of Perkin Elmer C30902SH at the any arbitrary overvoltage. The result also reinforces the point mentioned above, that increased overvoltage will result in increased dark counts.

### Dependence with temperature

With the APD set to an overvoltage of 12 V, the dark count rates are measured at temperatures ranging from  $-25^{\circ}\text{C}$  to  $25^{\circ}\text{C}$ , as shown in Figure 26 and 27.

It is observed that the dark count rate rises exponentially with temperature. This suggests that to lower the primary dark count, the device should be cooled as much as possible. However, the probability of afterpulsing effect increases with lower temperature operation [18] for the detrap time of the charge carriers increase exponentially with a reduction in temperature. Thus there is an optimum operating temperature for minimum dark counts and afterpulsing effects.

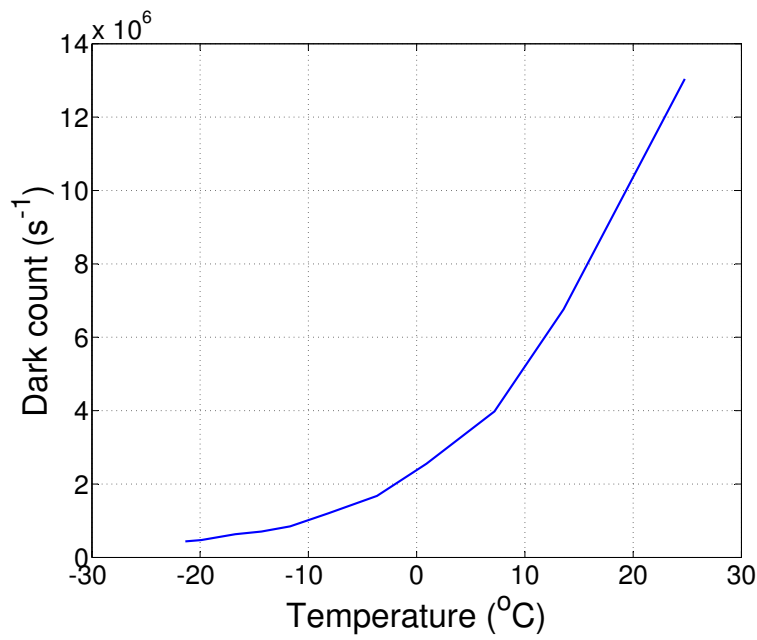


Figure 26: Dark count as a function of temperature for Perkin Elmer C30902SH.

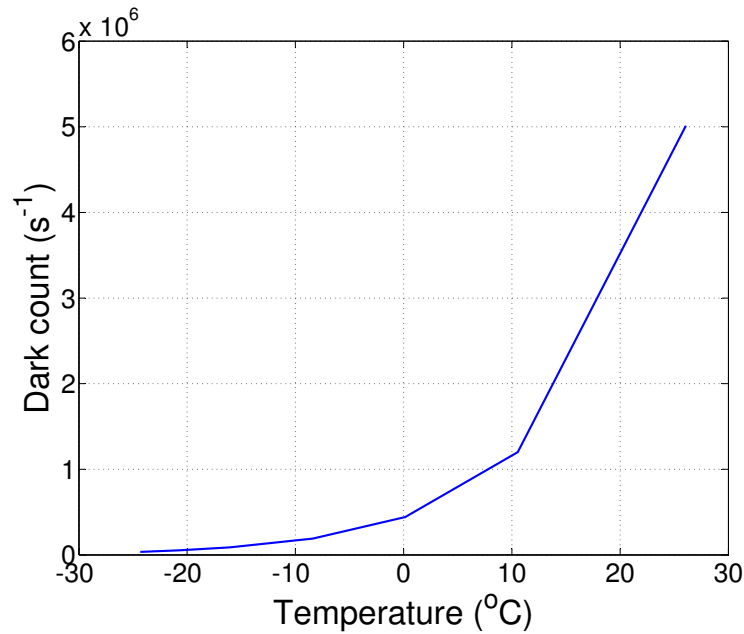


Figure 27: Dark count as a function of temperature for Laser Components SAP500.

### 3.3 Detection Efficiency

Detection efficiency is defined as the ratio of the actual number of counts detected to the expected number of counts assuming the detector was 100% efficient. It is important to find out this value for the measured efficiency of experiments which incorporates an APD, may be limited by the losses in the APDs used.

#### 3.3.1 Experimental setup

A light source of 810 nm is used throughout this measurement.

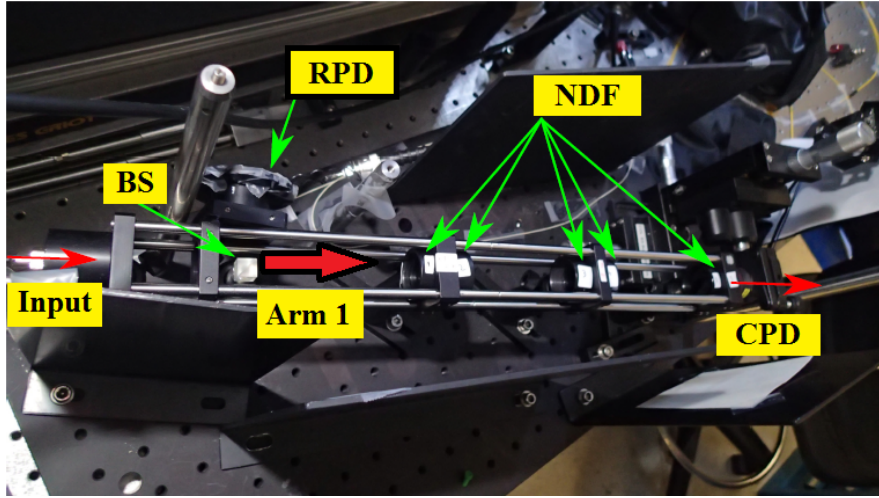


Figure 28: Setup for the efficiency measurement of APDs. A Hamamatsu S5107 silicon photodiode is used for the calibrated photodiode (CPD) and reference photodiode (RPD), which are bolometrically calibrated. BS is a calibrated beam splitter, with two output arms. Arm 1 is attenuated by neutral density (ND) filters and coupled to the test APD. Arm 2 is used as a reference for the input power.

Before proceeding with the efficiency measurements, we must first calibrate the losses in the other optical components we use.

#### Calibration of beam splitting ratio

The first step is to calibrate the beam splitter (BS) splitting ratio. With no filters in place, we used two calibrated photodiodes (CPD and RPD) on each output of the BS and measure the respective amount of current detected. The splitting ratio (SR) is determined by

$$SR = \frac{I_{CPD}}{I_{RPD}} \quad (7)$$

## Calibration of neutral density filters

To achieve single photon detection, neutral density filters were used to attenuate a collimated beam of power  $9 \mu\text{W}$  below the saturation limit of the APD. The attenuation of the ND filters is dependent on its thickness and angle placed with respect to the laser beam. The ND filters used were not AR coated resulting in a reflection from each filter surface. If the ND filters were placed perpendicular to the beam, it will cause an increase in the net transmission as compared to the filters calibrated individually, this is due to multiple back reflections creating an etalon-like effect, as illustrated in Figure 29.

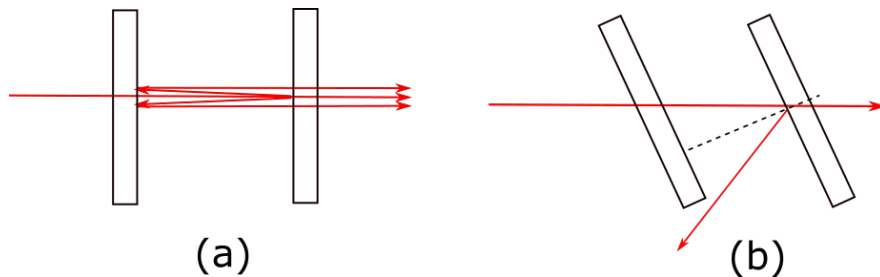


Figure 29: (a) ND filters placed perpendicular to the beam, resulting in multiple back reflections which increases the overall transmission. (b) ND filters placed at an angle to the beam, resulting in reflections directed out of the filters.

To mitigate this undesired effect, each ND filter was placed at an angle with respect to the beam. This is achieved by tilting the beam splitter (BS) such that the laser beam is incident onto the ND filters at an angle.

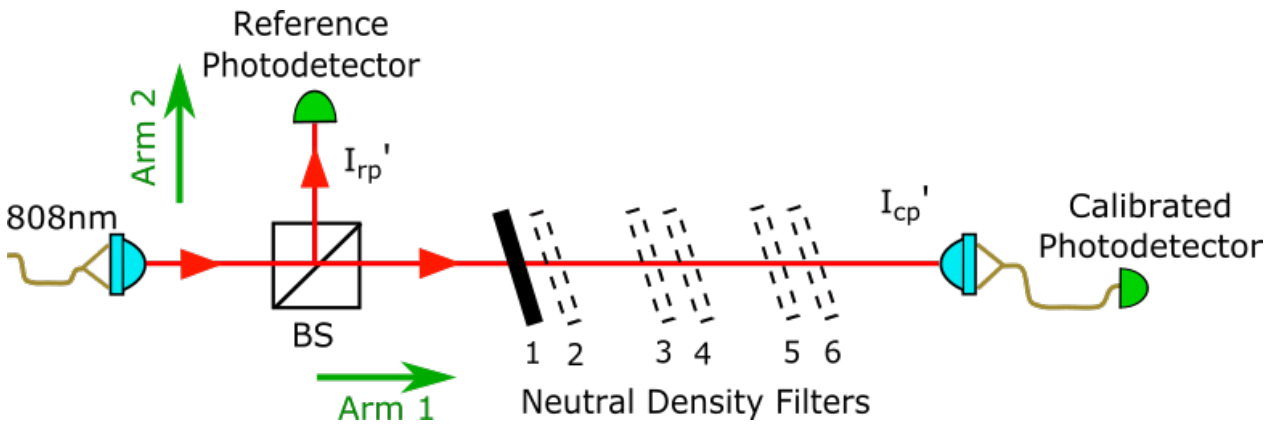


Figure 30: Setup for calibration of neutral density filters. The cage system is made up of short SM1 tubes (from Thorlabs) which serves as holders for the ND filters.

With the CPD placed at arm 1, the power of the transmitted beam after each single ND filter was measured. The RPD at arm 2 also measures the output of the other of the BS. A new splitting

ratio ( $SR'$ ) is thus obtained. The transmission factor ( $T_n$ ) of the beam after passing through the filter can be determined by

$$T_n = \frac{SR'}{SR} \quad (8)$$

In order to prove the absence of etalon-like effect due to filters placed nearby one other, we also measured the transmission after passing through both filters compared to the filters placed alone.

Filters	Transmission	Uncertainty
1	0.326	0.004
2	0.00858	0.00008
3	0.0374	0.0004
4	0.161	0.001
5	0.00160	0.00002
6	0.00277	0.00002
1,2	0.00281	0.00002
3,4	0.00582	0.00003
5,6	0.00002	0.00002

Figure 31: Results of transmission of filters. Filter 1,2 represents the transmission measured when both filter 1 and 2 are mounted.

Multiplying the transmission values of filter 1 and 2 together, we obtained a transmission value of  $0.00279 \pm 0.00004$ , which is the same as the transmission value obtained when filters 1 and 2 are mounted at the same time, taking into account the uncertainty. Repeating the same step for the other filter combinations, we achieved similar results. Thus, we confirmed the absence of an etalon-like effect caused by pairs of nearby ND filters. In addition, the total transmission factor ( $T$ ) of the ND filters is just a multiplication of all the respective  $T_n$  where

$$T = \prod_{n=1}^6 T_n \quad (9)$$

### Efficiency measurement

With all the ND filters mounted, the arm 1 output is now coupled to the APD and its NIM output was connected to the USB counter<sup>3</sup> unit. The arm 2 is coupled to the RPD which is used to monitor the power going into the APD. Before initiating the measurement, the fibre coupling is optimised again to compensate for any beam deviation due to the mounting of ND filters.

---

<sup>3</sup>The USB counter unit is a board with three TTL and NIM compatible inputs. It measures the number of counts detected by the APD.

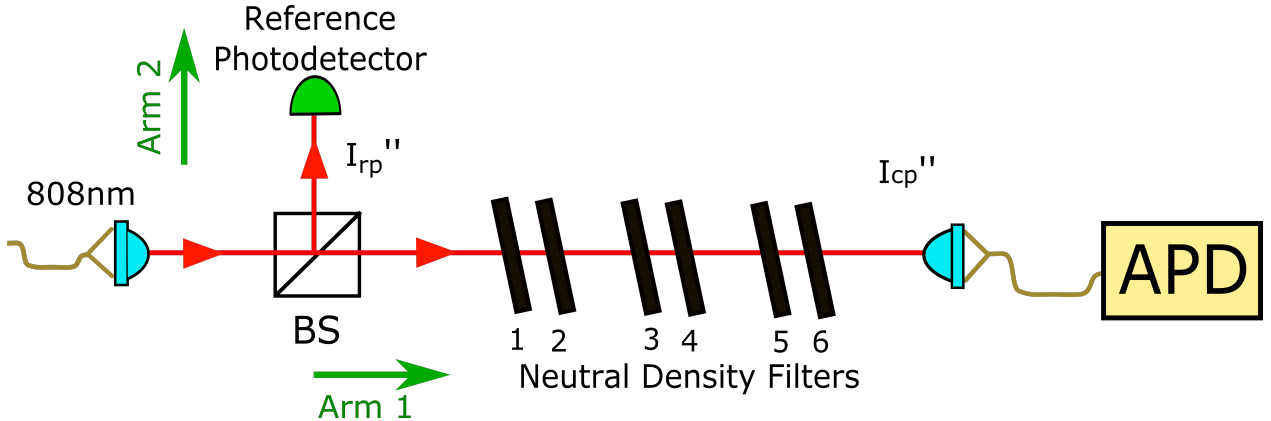


Figure 32: Setup for efficiency measurement

With the values of SR, T,  $I_{RPD}$ , and the sensitivity (s) of the RPD, the power incident onto the APD ( $P_{in}$ ) can be determined by

$$P_{in} = \frac{I}{s}(SR)T \quad (10)$$

Subsequently, the number of photons incident onto the APD per second (count<sub>in</sub>) can be obtained by

$$\text{count}_{in} = \frac{P_{in}}{\text{Energy of 1 photon}} \quad (11)$$

The experiment is then repeated for dark counts measurement at the respective APD operating conditions. Finally, with the number of counts and dark counts detected by the dt302 (count<sub>out</sub>), the efficiency (%) of the APD can be achieved by

$$\text{Efficiency} = \frac{\text{count}_{out} - \text{count}_{dark}}{\text{count}_{in}} \times 100\% \quad (12)$$

### 3.3.2 Dependence with overvoltage

Similar to the measurement in Chapter 3.2, the APD is in addition attached to the setup shown in Figure 12. With the APD set to the respective operating temperatures as shown in Figure 33 and 34, the efficiency of the APD is measured over a range of 30V overvoltage in steps of 3V. The overvoltage is set by varying the amount of biased voltage sent into the APD through the controllable voltage source.

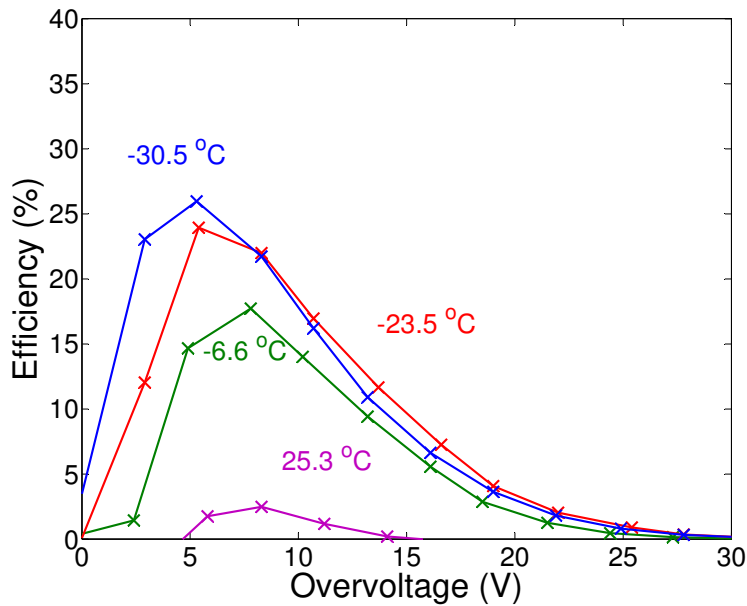


Figure 33: Efficiency as a function of overvoltage for Perkin Elmer C30902SH. The efficiency values have been accounted for dark counts.

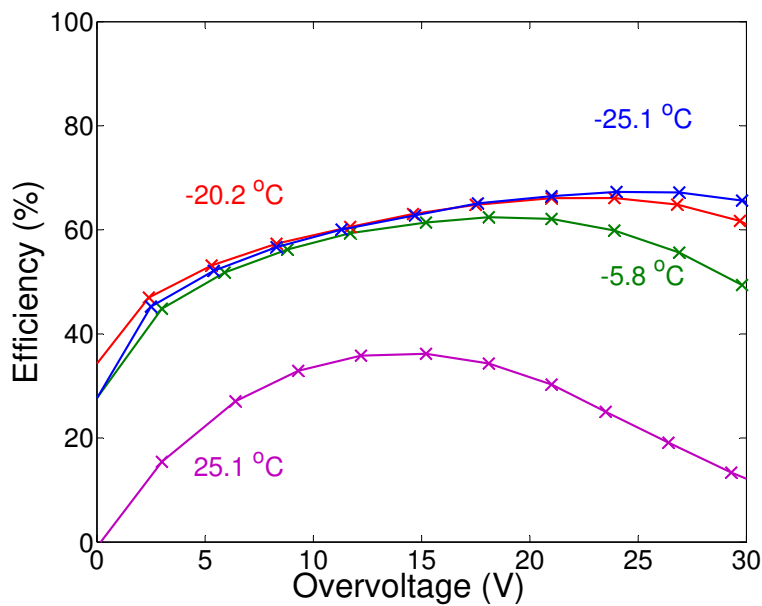


Figure 34: Efficiency as a function of overvoltage for Laser Component SAP500. The efficiency values have been accounted for dark counts.

From the results, we can conclude that Laser Component SAP500 has a much higher detection

efficiency than Perkin Elmer C30902SH. It is also observed that in the case of Perkin Elmer C30902SH, a higher overvoltage does not necessarily mean a higher efficiency - the optimum overvoltage at any temperature is around 5 to 10V. For the case of Laser Component SAP500, efficiency is seen to drop at a relatively much higher overvoltage - the optimum overvoltage should be around 25V. In addition, we see that in general, detection efficiency is higher at lower temperatures - possibly due to lesser dark pulses caused by thermal energy.

### 3.3.3 Dependence with count rate

In this section, we investigate the efficiency of the commercial APDs at varying incident count rates. In this context, the count rate is the number of photons incident onto the APD per second - the higher the incident power, the higher the count rate. Since the light source is a polarised laser light, the count rate is varied by polarizing the light to vary the incident power.

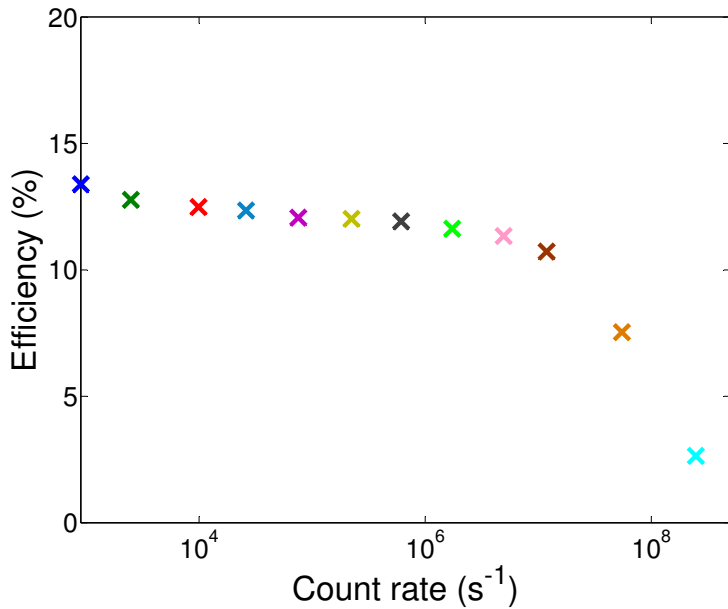


Figure 35: Efficiency as a function of count rate for MPD PD-050-CTD-FC. The efficiency values are accounted for dark counts.

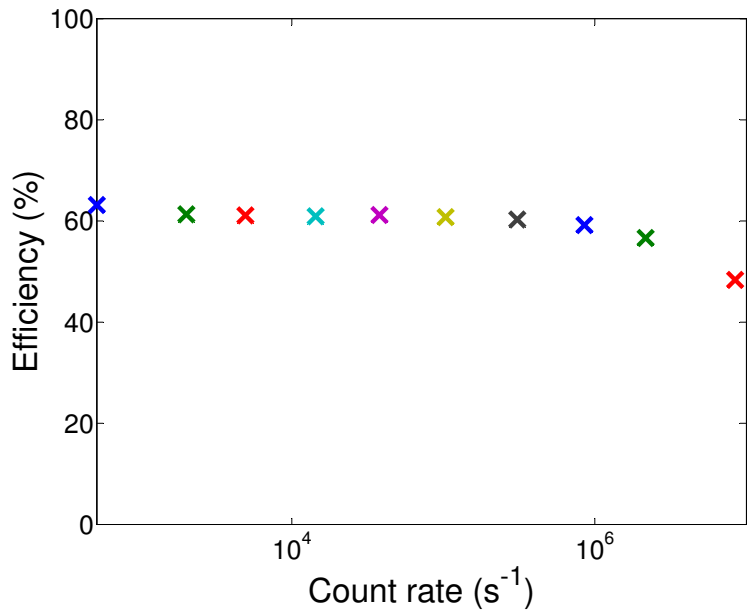


Figure 36: Efficiency as a function of count rate for Perkin Elmer SPCM-AQR-15.  
The efficiency values are accounted for dark counts.

From the results, it is observed that Perkin Elmer SPCM-AQR-15 has a much higher efficiency than MPD PD-050-CTD-FC. For both APDs, the detected photon count decreases at higher incoming light levels. The count rate at which the efficiency starts to decrease is called the saturation point. Both APDs saturates at count rates of order  $10^7$ .

## 3.4 Timing Jitter

In many experimental methods such as time resolved spectroscopy or quantum communications, precise timing of photon arrival is essential. Timing jitter is defined as the statistical fluctuations of the time interval between the arrival photon at the detector and the output pulse leading edge [19].

### 3.4.1 Experimental setup

Timing jitter measurements require short optical pulses as timing references. Hence, a light source from a Ti:Sapphire laser is used throughout this measurement. The laser has a wavelength of 770 nm<sup>4</sup>, with a pulse duration of approximately 100 fs, and a repetition rate of 76 MHz. The input power of the laser is approximately 4 mW.

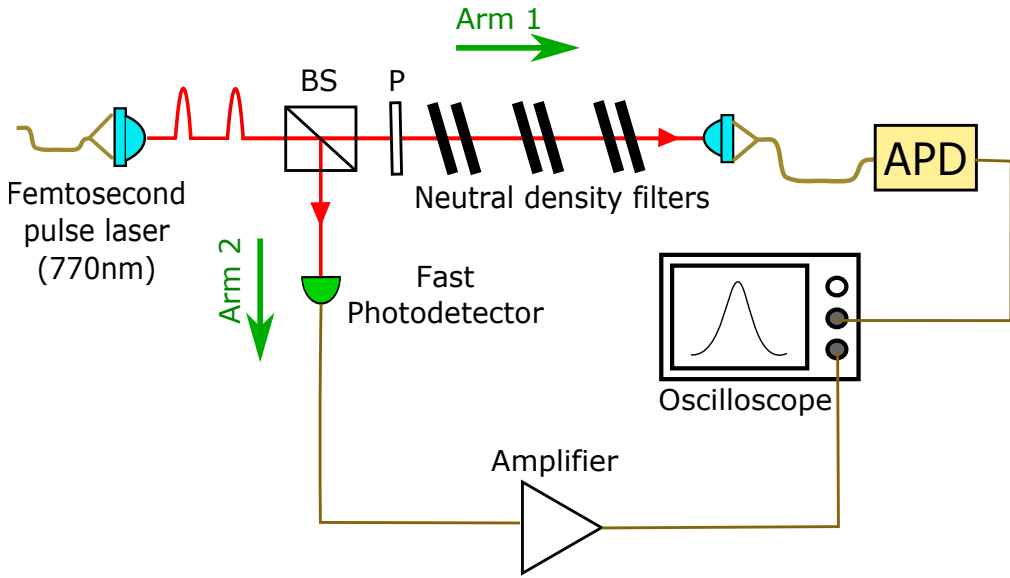


Figure 37: Setup for jitter measurement

Similar to the set up for efficiency measurement, calibrated neutral filters are placed at arm 1 to attenuate the light to single photon level. In addition to the NDFs, a polarizer is placed along arm 1 to allow fine variation of the intensity of light. Light after passing through the NDFs is then coupled into the APD through a multimode fibre. The APD then outputs a NIM pulse to the oscilloscope (WaveRunner 640Zi). A fast photodetector (Hamamatsu G4176, rise time 30 ps) is placed at arm 2, and its output signal is amplified by a chain of amplifiers (3 x Minicircuits MAR-6, total amplification  $\sim 60$  dB) resulting in an output signal amplitude of approximately 0.5V (see Figure 38) on the oscilloscope.

<sup>4</sup>This choice of wavelength is up to the lab that we borrow the femtosecond laser from.

The oscilloscope is set to the qualify-trigger mode such that it qualifies on the fast photodiode pulse and triggers on the APD NIM pulse, and sets a measurement on the time delay between the two pulses at half of their heights as shown in Figure 38. To reduce the dead time between acquisitions, the time between the qualifier and trigger is set to below 10 to 20 ns, in consideration of the path length difference. The sequence mode is turned on thus further reducing the dead time between triggers to less than 1  $\mu$ s.

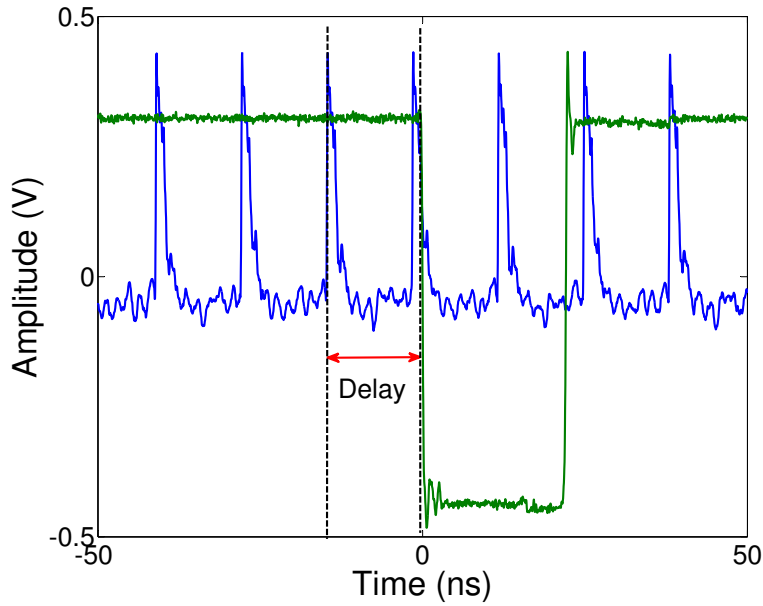


Figure 38: Time delay between the fast photodiode signal pulse (blue) and the APD NIM pulse (green).

The oscilloscope then provides a histogram of the time delay between the two signals. The data is sorted into 5000 bins, each 1 ps wide.

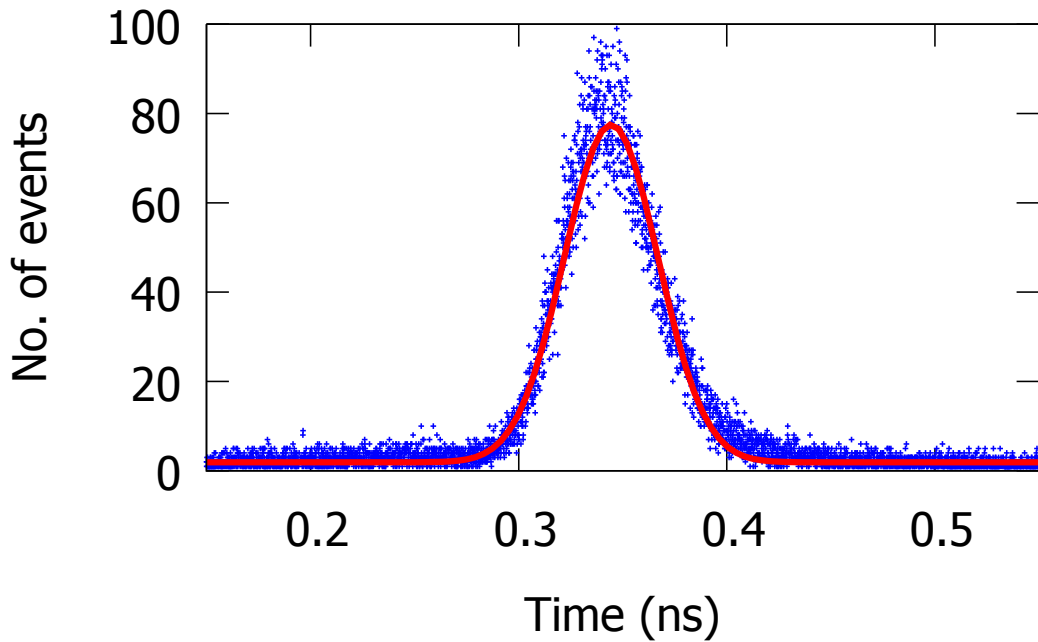


Figure 39: Histogram plot for Perkin Elmer C30902SH at standard operating temperature of -25 °C and overvoltage of 12V, with incident count rate of 10 kHz. The blue data points represent the number of events happening at the respective time delays, and the red line is a Gaussian fit of the data.

A Gaussian fit is then done on the histogram plot, and the resulting full width at half maximum (FWHM) of the fit is the timing jitter of the APD. The peak of the fit corresponds to the average time delay between the two pulses.

### 3.4.2 Dependence with count rate

First, we investigate the dependence of the timing jitter on incident count rate. The incident count rate is varied by reducing the intensity of incident light using the polarizer. Here, we measured the dependence of timing jitter on incident count rate of the Perkin Elmer C30902SH.

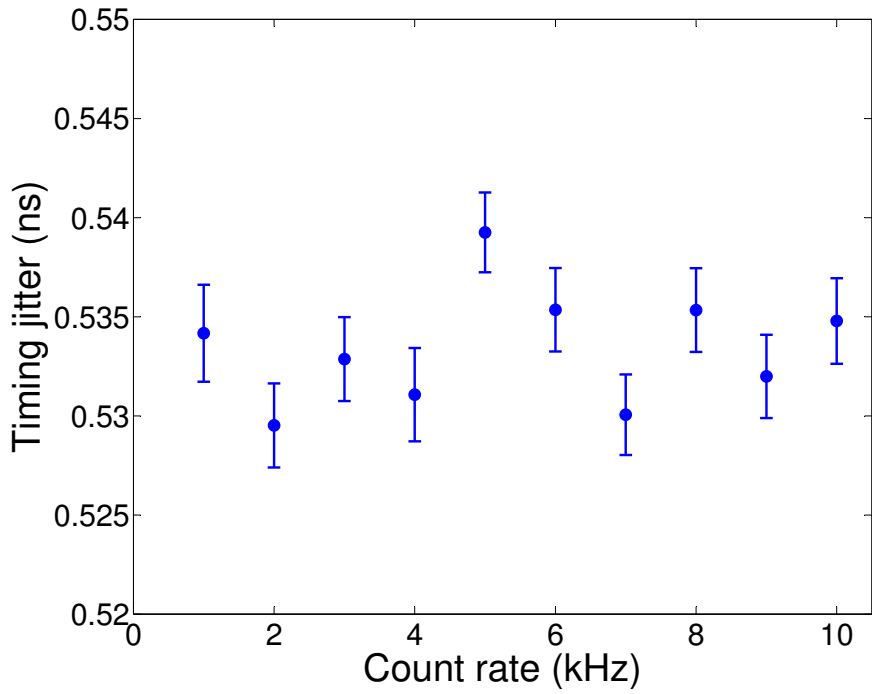


Figure 40: Timing jitter as a function of incident count rate for Perkin Elmer C30902SH.

The results shows that timing jitter does not vary significantly with count rates up to 10 kHz.

### 3.4.3 Dependence with overvoltage and temperature

The measurement then continues to investigate the dependence of timing jitter on the overvoltage and temperature of the APD. The overvoltage and temperature is varied by adjusting the high voltage and temperature control directly from the APD circuit board as shown in Figure 11.

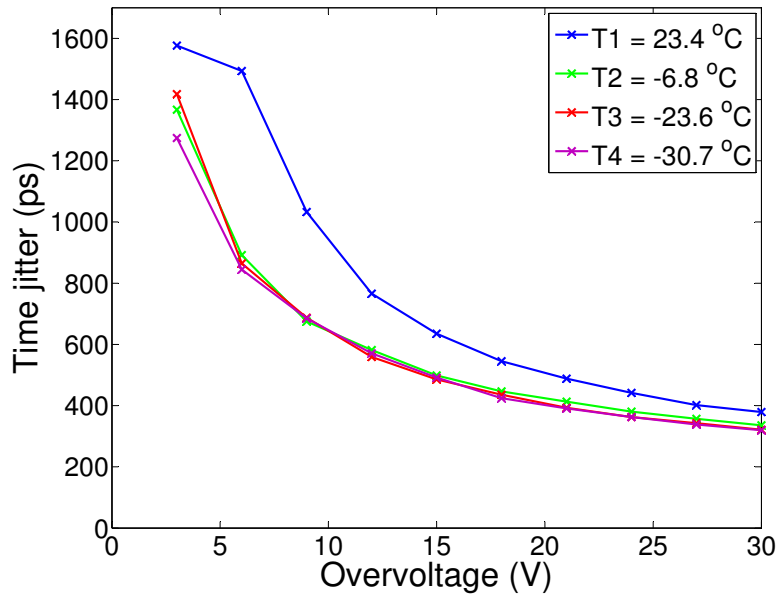


Figure 41: Timing jitter as a function of overvoltage for Perkin Elmer C30902SH.

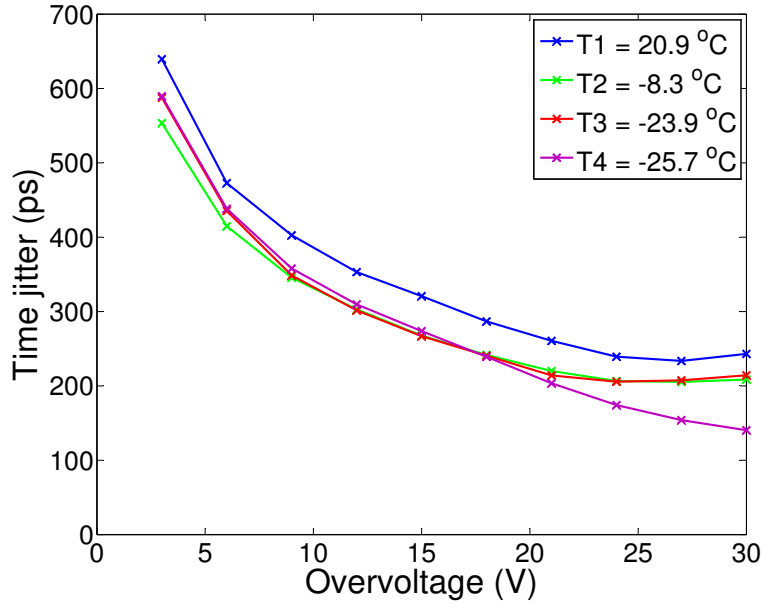


Figure 42: Timing jitter as a function of overvoltage for Laser Components SAP500.

It can be deduced from the results that the timing jitter does not have a strong dependence on temperature. However, temperature T1 of Perkin Elmer C30902SH produces a distinct higher timing jitter curve. This is possibly due to a higher signal-to-noise ratio because of its high tem-

perature. In general, timing jitter decreases with increasing overvoltage. In addition, comparing Figure 41 and 42, Laser Components SAP500 generally offers a better timing jitter than Perkin Elmer C30902SH.

Another interesting result is that the average time delay is in fact dependent on overvoltage. This can be seen in Figure 43 and 44, where the centre of the histogram plots shifts to the left with increasing overvoltage. This phenomena could be due to a faster photon detection by the APD caused by the high electric field across the depletion region at high overvoltages.

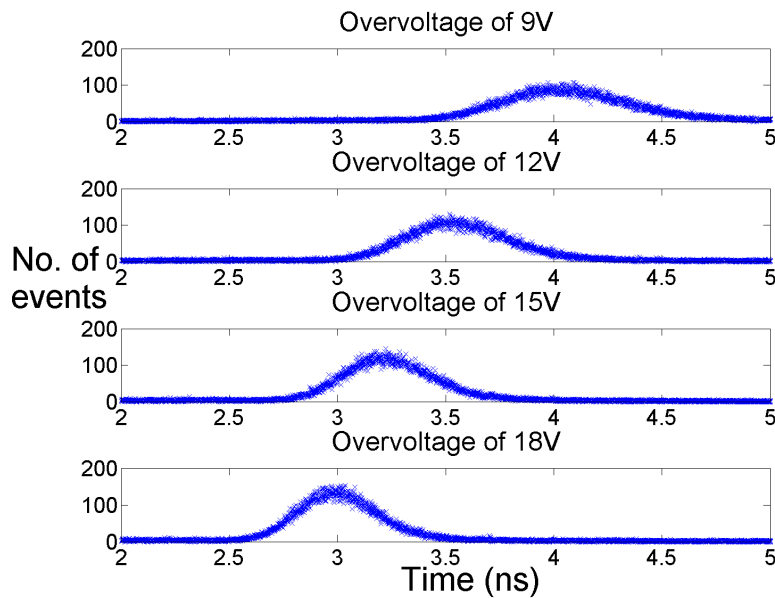


Figure 43: Histogram of time delay as a function of time for Perkin Elmer C30902SH. The APD is set to a temperature of  $-23.6^{\circ}\text{C}$ , with a count rate of 50 000 cps.

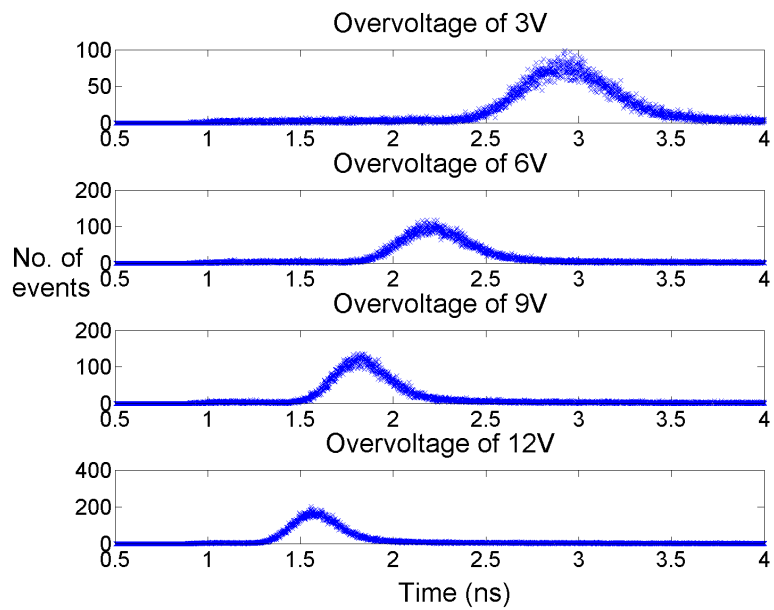


Figure 44: Histogram of time delay as a function of time for Laser Components SAP500. The APD is set to a temperature of  $-25.7^{\circ}\text{C}$ , with a count rate of 50 000 cps.

## 3.5 Breakdown Flash Probability

The breakdown flash is a discharge of light due to the recombination of charge carriers with the bulk carriers, and do not contribute to the current flow. These events may cause false readings in photon correlation experiments such as those used in single atom spectroscopy and single photon interferometry experiments where a breakdown flash off one detector may be observed in the other detector.

### 3.5.1 Experimental setup

To measure the breakdown flash off one APD, two identical APDs are connected to one another by a multimode fibre while being exposed to ambient light, such that its breakdown flash is detected by the other. The coincidence events of the two APDs are collected by and their time differences  $t_2 - t_1$  are histogrammed by the timestamp as shown in Figure 46.

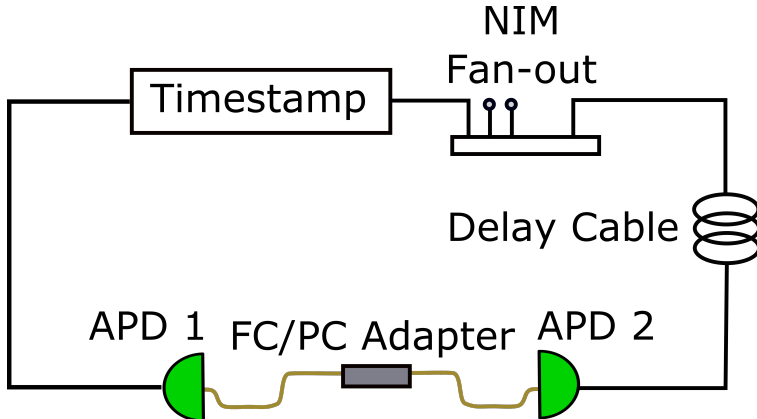


Figure 45: Setup for measuring breakdown flash of MPD PDM-050-CTC-FC. The two APDs are connected to each other by a FC/PC adapter, through a multimode fibre,. A delay cable is used due to electronic delays of the time stamp. A NIM fan-out is used to "clean out" the signal due to signal degradation when travelling through the long delay cable.

### 3.5.2 Quantifying Breakdown Flash Probability

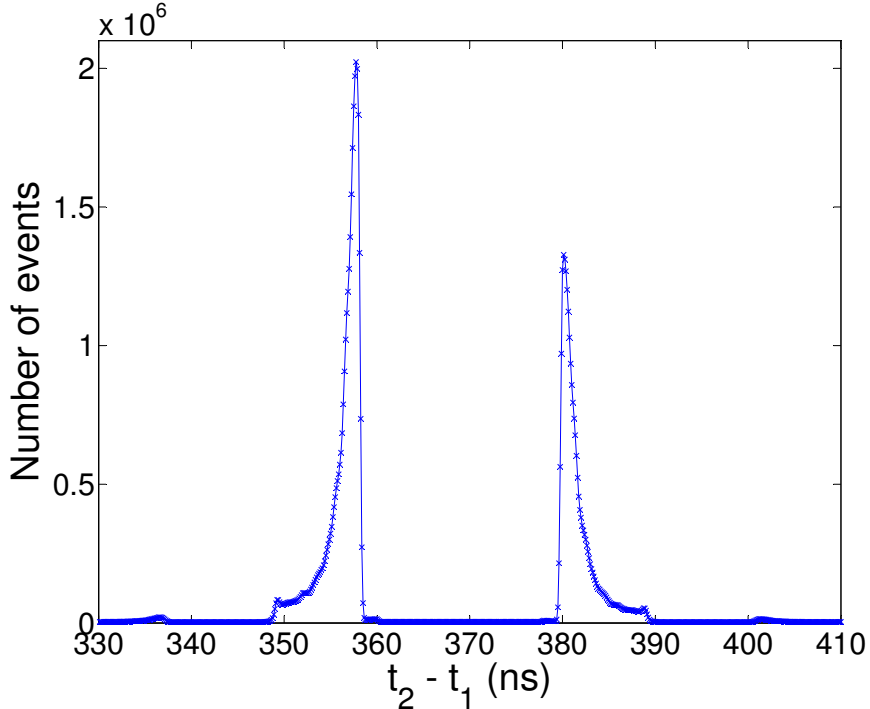


Figure 46: A histogram of the coincidence measurement between two APDs as a function of the time delay between the detection events. The right peak corresponds to photons emitted by APD 1 seen by APD 2. The asymmetry is due to the APDs not receiving the same amount of ambient light. The smalls bumps (at approximately 335 ns and 400 ns) are due to secondary breakdown flash emission.

We define the breakdown flash probability as the ratio of number of coincidence events to the total number of events detected by the APD.

$$\text{Breakdown Flash Probability} = \frac{\text{Total no. of coincidence events}}{\text{Total number of events}} \quad (13)$$

The total number of coincidence events can be achieved by integrating the area under the respective peaks as shown in Figure 46.

The detected breakdown flash probability of the two MPDs are calculated to be 0.19 and 0.17 respectively. These values are not corrected for the detection efficiency; to do so would require a knowledge of the spectrum of the breakdown flash [20].

## 4 Conclusion and outlook

In this thesis, we have successfully evaluated the performance of two types of passively quenched APDs. The results show that the Laser Components SAP500 displays better performance than Perkin Elmer C30902SH in all of the characterised parameters: a lower breakdown voltage, higher gain, lower dark count rate, higher efficiency at 808 nm, and shorter timing jitter. For the actively quenched APDs, the Perkin Elmer SPCM-AQR-15 has a higher efficiency at 808 nm than the MPD PD-050-CTD-FC, but also a larger timing jitter. Overall, the MPD is most suited for experiments occurring on extremely short time scales, while the Laser Components SAP500 would be a better choice for experiments requiring a high detection efficiency.

However, the characterisation of the breakdown flash probability is not complete, as we have only measured it for the MPD detector. We also attempted to do so for the Perkin Elmer SPCM-AQR-15, but were unable to extract meaningful result due to spurious artefacts in the measurements. Therefore, the project should proceed to complete this characterisation for the other APDs. Moreover, to correct the breakdown flash probability for detection efficiencies, we should also measure the breakdown flash spectrum, which can be done by a spectrometer.

Finally, with a comprehensive set of measurement methods in place, we can extend the characterisation to other types of APDs.

## References

- [1] A. Pais, "Einstein and the quantum theory," *Reviews of Modern Physics*, vol. 51, no. 4, p. 863, 1979.
- [2] J. D. Norton, "How einstein changed the way we think about science."
- [3] E. Mbakop, "A historical perspective on quantum physics and its impact on society," Ph.D. dissertation, WORCESTER POLYTECHNIC INSTITUTE, 2009.
- [4] D. Renker, "Photosensors," *Nuclear Instruments and Methods in Physics Research Section A: Accelerators, Spectrometers, Detectors and Associated Equipment*, vol. 527, no. 1, pp. 15–20, 2004.
- [5] Hamamatsu, "Photomultiplier tubes basics and applications."
- [6] E. Hergert, "Detectors: Guideposts on the road to selection," *Photonics Design and Applications Handbook*, pp. H110–H113, 2001.
- [7] C. Bennett, G. Brassard, and A. Ekert, "Quantum cryptography," in *Progress in Atomic physics Neutrinos and Gravitation, proceedings of the XXVIIth Rencontre de Moriond Series: Moriond Workshops, held January, 1992*, p. 371.
- [8] R. H. Hadfield, "Single-photon detectors for optical quantum information applications," *Nature photonics*, vol. 3, no. 12, pp. 696–705, 2009.
- [9] N. Gisin, G. Ribordy, W. Tittel, and H. Zbinden, "Quantum cryptography," *Reviews of modern physics*, vol. 74, no. 1, p. 145, 2002.
- [10] G. Brassard, N. Lütkenhaus, T. Mor, and B. C. Sanders, "Limitations on practical quantum cryptography," *Physical Review Letters*, vol. 85, no. 6, p. 1330, 2000.
- [11] V. Leong, S. Kosen, B. Srivathsan, G. K. Gulati, A. Cerè, and C. Kurtsiefer, "Hong-ou-mandel interference between triggered and heralded single photons from separate atomic systems," *Physical Review A*, vol. 91, no. 6, p. 063829, 2015.
- [12] P. Tan, C. Chia, W. Han, A. Chan, and C. Kurtsiefer, "Null stellar intensity interferometry," *Proceedings of the International Astronomical Union*, vol. 8, no. S293, pp. 420–422, 2012.
- [13] B. A. SAMRAT, K. SAMBASIVARAO, and K. RAGHUNATH, "Performance characteristics of detector devices used in lidar system."

- [14] R. G. Brown, K. D. Ridley, and J. G. Rarity, "Characterization of silicon avalanche photodiodes for photon correlation measurements. 1: Passive quenching," *Applied Optics*, vol. 25, no. 22, pp. 4122–4126, 1986.
- [15] J. Y. Cheung, C. J. Chunnillall, P. J. Thomas, J. R. Mountford, and N. P. Fox, "Photon-counting: measurement challenges," in *International Congress on Optics and Optoelectronics*. International Society for Optics and Photonics, 2007, pp. 65 830G–65 830G.
- [16] M. Stipčević, H. Skenderović, and D. Gracin, "Characterization of a novel avalanche photodiode for single photon detection in vis-nir range," *Optics express*, vol. 18, no. 16, pp. 17 448–17 459, 2010.
- [17] S. Cova, M. Ghioni, A. Lacaita, C. Samori, and F. Zappa, "Avalanche photodiodes and quenching circuits for single-photon detection," *Applied optics*, vol. 35, no. 12, pp. 1956–1976, 1996.
- [18] Y. Kang, D. Bethune, W. Risk, and Y.-H. Lo, "Afterpulsing of single-photon avalanche photodetectors," in *Lasers and Electro-Optics Society, 2003. LEOS 2003. The 16th Annual Meeting of the IEEE*, vol. 2. IEEE, 2003, pp. 775–776.
- [19] C. Niclass, A. Rochas, P.-A. Besse, and E. Charbon, "Design and characterization of a cmos 3-d image sensor based on single photon avalanche diodes," *Solid-State Circuits, IEEE Journal of*, vol. 40, no. 9, pp. 1847–1854, 2005.
- [20] C. Kurtsiefer, P. Zarda, S. Mayer, and H. Weinfurter, "The breakdown flash of silicon avalanche photodiodes-back door for eavesdropper attacks?" *Journal of Modern Optics*, vol. 48, no. 13, pp. 2039–2047, 2001.